



HAL
open science

Structural control on shallow hydrogeochemical processes at Caviahue-Copahue Volcanic Complex (CCVC), Argentina

Daniele Tardani, Emilie Roulleau, Daniele L Pinti, Pamela Pérez-Flores, Linda Daniele, Martin Reich, Pablo Sanchez-Alfaro, Diego Morata, Luc Richard

► **To cite this version:**

Daniele Tardani, Emilie Roulleau, Daniele L Pinti, Pamela Pérez-Flores, Linda Daniele, et al.. Structural control on shallow hydrogeochemical processes at Caviahue-Copahue Volcanic Complex (CCVC), Argentina. *Journal of Volcanology and Geothermal Research*, 2021, 414, 10.1016/j.jvolgeores.2021.107228 . hal-03184971

HAL Id: hal-03184971

<https://hal.univ-reunion.fr/hal-03184971v1>

Submitted on 30 Mar 2021

HAL is a multi-disciplinary open access archive for the deposit and dissemination of scientific research documents, whether they are published or not. The documents may come from teaching and research institutions in France or abroad, or from public or private research centers.

L'archive ouverte pluridisciplinaire **HAL**, est destinée au dépôt et à la diffusion de documents scientifiques de niveau recherche, publiés ou non, émanant des établissements d'enseignement et de recherche français ou étrangers, des laboratoires publics ou privés.

1
2
3
4
5 1 **Structural control on shallow hydrogeochemical processes at**
6
7
8 2 **Caviahue-Copahue Volcanic Complex (CCVC), Argentina**
9

10 3 Daniele TARDANI^{1,2*}, Emilie ROULLEAU^{3,4}, Daniele L. PINTI^{5,6,7}, Pamela PERÉZ-FLÓRES⁸,
11
12 4 Linda DANIELE^{2,9}, Martin REICH^{2,9}, Pablo SÁNCHEZ^{1,2}, Diego MORATA^{2,9}, Luc RICHARD⁵
13
14
15 5

16
17
18 6 1 – Instituto de Ciencias de la Tierra, Universidad Austral de Chile, Valdivia, Chile
19

20 7 2 – Andean Geothermal Center of Excellence (CEGA), Universidad de Chile, Santiago, Chile
21

22 8 3 – Stratagem974, Sainte Clotilde, La Réunion, France
23

24 9 4 – Université de La Réunion, Laboratoire Géosciences Réunion, F-97744 Saint Denis, France
25
26

27 10 5 – GEOTOP and Département des Sciences de la Terre et de l'Atmosphère, Université du Québec
28
29 11 à Montréal, Montréal QC, Canada
30

31
32 12 6 – Key Laboratory of Petroleum Resources, Gansu Province, Northwest Institute of Eco-
33
34 13 Environment and Resources, Chinese Academy of Sciences, Lanzhou 730000, China
35
36

37 14 7 – Gansu Talent and Intelligence Center for Remediation of Closed and Old Deposits, Lanzhou
38
39 15 730000, China
40
41

42 16 8 – Consultoria e Investigación Geológico Ambiental Ltda. Huasco. Chile
43

44 17 9 – Department of Geology, Facultad de Ciencias Físicas y Matemáticas. Universidad de Chile,
45
46 18 8370450 Santiago, Chile
47
48

49 19 * Corresponding author: E-mail: daniele.tardani@uach.cl
50
51

52 20 Keywords: Helium isotopes; stable isotopes; radiocarbon; tritium; strontium isotopes; Copahue
53
54 21 volcano.
55
56

57 22 Revised version to *Journal of Volcanology and Geothermal Research*
58

59 23 Abstract words: 319; Text words: 6921; References = 64; Figures = 8; Tables = 2
60
61

1
2
3
4 **Abstract**

5
6 25 The Caviahue-Copahue Volcanic Complex (CCVC) hosts one of Argentina's most
7
8
9 26 important geothermal systems. To provide new insights into origin, circulation, and residence time
10
11 27 of fluids, the chemical and isotopic composition ($^3\text{He}/^4\text{He}$, $\delta^2\text{H}-\delta^{18}\text{O}$ in H_2O ; $\delta^{13}\text{C}-\delta^{18}\text{O}$ in CO_2 ;
12
13
14 28 $^{87}\text{Sr}/^{86}\text{Sr}$) of thermal waters was measured together with the ^3H and ^{14}C activities. Water samples
15
16 29 were collected from hot springs (LM, TC, LMM, CB and AF) representing the five major thermal
17
18
19 30 zones of the CCVC and assumed to be steam-heated meteoric waters, and a well condensate (COP-
20
21 31 2). The LMM, CB, and AF chemical composition and $^{87}\text{Sr}/^{86}\text{Sr}$ ratios show that water chemistry is
22
23 32 acquired locally from exchange with volcanic rocks (Sr, SiO_2 , among others) and from steam (H_2S).
24
25
26 33 Two surface geothermal manifestations (LM and TC), along with the well condensate, COP-2,
27
28
29 34 contain a higher contribution of deep-originating fluids, with $^{87}\text{Sr}/^{86}\text{Sr}$ indicating possible
30
31 35 contribution from deep-seated granitoids or sediments from the underlying basement.
32
33 36 Radiocarbon-based residence times indicate ages ranging between 13,540 and 17,520 yrs BP,
34
35
36 37 representing the minimum age for the geothermal reservoir waters. Tritium is mainly absent in hot
37
38
39 38 spring waters except for LMM and CB where the activity is close to the detection limit. This
40
41 39 indicates a minimum age older than 70 yrs for the water circulating in the shallow circuit. This
42
43 40 result suggests that shallow meteoric water have a more complex and/or deeper circuit, resulting
44
45 41 in older residence times. Helium isotopes in the CCVC span a wide range, from a pure mantle-
46
47
48 42 derived value, of 8.35Ra, to a more crustal radiogenic signature, of 4.6Ra. The spatial variation is
49
50
51 43 explained by associating the geochemical data with the geological context, which includes the
52
53 44 distribution of fault-fracture meshes and different sources of magmatic volatiles underlying the
54
55 45 Copahue volcano. The first order control on helium isotope signatures observed in this study seems
56
57
58 46 to be dominated by the degree of crustal assimilation of the magmatic sources, which is in turn
59
60 47 controlled by the local arrays of faults.

1
2
3
4
5
6
7
8
9
10
11
12
13
14
15
16
17
18
19
20
21
22
23
24
25
26
27
28
29
30
31
32
33
34
35
36
37
38
39
40
41
42
43
44
45
46
47
48
49
50
51
52
53
54
55
56
57
58
59
60
61
62
63
64
65

48 **1. INTRODUCTION**

49 The Copahue stratovolcano, part of the Caviahue-Copahue Volcanic Complex (CCVC), is
50 an active volcano that hosts a high-enthalpy geothermal system (JICA, 1992) that represents a
51 promising resource for geothermal energy in Argentina (Barcelona et al., 2020). The CCVC is
52 located in the Southern Volcanic Zone (SVZ, 33 - 46 ° S) of the Andes, at the northern termination
53 of the intra-arc, strike-slip, Liquiñe-Ofqui Fault System (LOFS). Here, a trans-tensional-NE
54 transfer zone is developed, linking the LOFS and the Antifñir-Copahue Fault System (e.g. Sielfeld
55 et al, 2017).

56 The geothermal area of interest lies to the north and northwest of the Copahue volcanic
57 edifice, with several surface emissions including fumaroles, bubbling pools, mud pools and thermal
58 springs, which are spatially associated with local extensional faults which act as fluid preferential
59 pathways (Nakanishi et al., 1995; Melnick et al., 2006; Barcelona et al., 2019). The area has been
60 studied extensively over the last thirty years, and, in the early 1990s, the Japanese International
61 Cooperation Agency (JICA) carried out a deep drilling campaign and a feasibility study for
62 developing a high-enthalpy geothermal field. Renewed interest in studying the processes
63 controlling this hypothermal system was driven by the anomalous volcanic unrest of the Copahue
64 volcano during the 2012-2016 period and by the possibility of developing potential geothermal
65 resources in the Andean region (Barcelona et al., 2020). In recent years, several studies have
66 focused on the geochemistry of the Copahue volcanic-hydrothermal system and its CO₂ surface
67 degassing (Agusto et al., 2013; Agusto and Varekamp, 2016; Chiodini et al., 2015; Roulleau et al.,
68 2016, 2017; Tassi et al., 2017; Lamberti et al., 2019). These studies have improved our
69 understanding of the structural factors controlling the hydrothermal activity, and have provided
70 crucial information to refine the conceptual model of the local fault-fracture hydraulic architecture
71 in the Copahue geothermal system (Barcelona et al., 2019).

1
2
3
4 72 The goal of this study is to assess relevant processes acting in the hydrological system of
5
6 73 Copahue, as the residence time of fluids, hydrothermal fluid sources and circulation patterns. In
7
8
9 74 the present contribution are presented the first radiocarbon (^{14}C) activities together with strontium
10
11 75 ($^{87}\text{Sr}/^{86}\text{Sr}$) isotope data measured in geothermal water samples collected from five thermal pools
12
13
14 76 and a well steam condensate of the Copahue geothermal system. Together with new $\delta^2\text{H}$, $\delta^{18}\text{O}$,
15
16 77 $\delta^{13}\text{C}\text{-CO}_2$, $\delta^{18}\text{O}\text{-CO}_2$, ^3H , $^3\text{He}/^4\text{He}$, and $^4\text{He}/^{20}\text{Ne}$ data, they provide further insights into the
17
18
19 78 residence times of deep and shallow fluids, the water–rock interaction processes, and the structural
20
21 79 pathways that link the deep magmatic/geothermal system and the surface aquifers.
22
23
24 80

27 81 **2. GEOLOGICAL SETTING OF THE CCVC GEOTHERMAL SYSTEM**

28
29
30 82 The CCVC is located at 37.5°S and 71°W , at the border between Argentina and Chile in the
31
32 83 Southern Volcanic Zone of the Andes and is composed of the Caviahue caldera and the Copahue
33
34
35 84 stratovolcano (Fig. 1). The Caviahue caldera is a square-shaped depression of ca. $20\text{ km} \times 15\text{ km}$,
36
37 85 defined as a trans-tensional pull-apart intra-arc basin due to the NE-transition zone between LOFS
38
39
40 86 and the Copahue-Antiñir fault zone (Melnick et al., 2006).

41
42 87 The Copahue volcano is an active stratovolcano, situated on the western rim of the Caviahue
43
44 88 caldera. Volcanic activity at Copahue began ca. 1 Ma ago. Since the Upper Pleistocene, volcanic
45
46
47 89 activity has consisted mainly of andesitic lava flows and a few later-Holocene explosive episodes
48
49 90 of andesitic to trachydacitic composition (Linares et al., 1999).

50
51
52 91 The Copahue geothermal system has developed at the northeastern part of the Copahue
53
54 92 volcano, hosted in the Caviahue Caldera. The geothermal field mainly extends over the Copahue
55
56
57 93 Village Fault System (Figure 1), composed of a set of extensional $\sim\text{N}^\circ 60$ -striking faults – developed
58
59 94 in a structural block between the Trolope and Chanco-có WNW-striking faults (Bonali et al., 2016;
60
61
62
63
64
65

1
2
3
4
5
6
7
8
9
10
11
12
13
14
15
16
17
18
19
20
21
22
23
24
25
26
27
28
29
30
31
32
33
34
35
36
37
38
39
40
41
42
43
44
45
46
47
48
49
50
51
52
53
54
55
56
57
58
59
60
61
62
63
64
65

95 Barcelona et al., 2019; 2020) – which affect the ignimbrites of the Las Mellizas volcanic sequence
96 (JICA, 1992; Barcelona et al., 2020). Five active geothermal zones are recognized within the area,
97 with evident surface manifestations consisting of hot springs, boiling pools, bubbling pools, and
98 mud pools with temperatures of up to 96°C, and fumaroles that reach temperatures of up to 135°C
99 (Agusto et al., 2013). The five thermal zones of Las Maquinas (LM), Las Maquinitas (LMM),
100 Termas de Copahue (TC), Cabañita (CB), and Anfiteatro (AF) are located northeast of the volcano
101 and appear to be spatially associated with NE- and WNW-striking fault systems (Melnick et al.,
102 2006; Barcelona et al., 2019). The Chanco-có (CC) geothermal field is located on the northern
103 flank of the volcano, in the WNW-striking Chanco-có Fault, in close proximity to the volcanic–
104 hydrothermal system. The Pucon-Mahuida (PM) bubbling gas manifestation lies on the southern
105 flank of Copahue volcano (Fig. 1). The complex fault systems interaction, under an extensional
106 stress field, defines a NE-striking fault with high dilation tendency, while the WNW-striking faults
107 are related to medium to low dilation tendency (Barcelona et al., 2019). This fault architecture
108 controls the permeability and pathways of the hydrothermal fluids and meteoric water, and their
109 isotopic and chemical variations (Barcelona et al., 2019).

110 The geothermal system at depth is characterized by a layered reservoir containing a shallow
111 steam cap at 1000 m depth and a liquid-dominated level below 2000 m depth (Barcelona et al.,
112 2019). The reservoir is located within Pliocene volcanic and volcanoclastic rocks, with a
113 temperature higher than 270°C (JICA, 1992; Agusto et al., 2013; Barcelona et al., 2019; 2020). The
114 reservoir has pervasive propylitic alteration. The upper thermal boundary includes a clay cap,
115 which correlates with the andesitic deposits of the Las Mellizas Formation, affected by an advanced
116 argillic alteration (Mas et al., 1995; Barcelona et al., 2019; 2020).

117 The surface geothermal pools in the geothermal/fumarolic areas around the volcano edifice
118 are assumed to be steam-heated meteoric waters, partially evaporated as those in the crater lake, as

1
2
3
4 119 indicated by the water stable isotope composition (e.g., Agosto et al., 2013; Agosto and Varekamp,
5
6 120 2016). The stable isotopic composition of the local meteoric water endmember is assumed to be
7
8
9 121 $\delta^2\text{H} = -80 \pm 5 \text{‰}$ and $\delta^{18}\text{O} = -11.2 \pm 0.4 \text{‰}$ vs SMOW (Panarello, 2002) which is somehow in between
10
11 122 the theoretical values for precipitations calculated using the Online Isotope Precipitation Calculator
12
13
14 123 (OIPC; Bowen, 2017) at the 2965 m Copahue summit ($\delta^2\text{H} = -90 \text{‰}$, $\delta^{18}\text{O} = -12.6 \text{‰}$) and at the
15
16 124 base of the edifice at the town of Caviahue ($\delta^2\text{H} = -70 \text{‰}$, $\delta^{18}\text{O} = -9.9 \text{‰}$) (Agosto and Varekamp,
17
18
19 125 2016). The hydrological model developed by Agosto et al. (2013) suggests that the volcanic-
20
21 126 hydrothermal system underlying Copahue active crater consists of glacial meltwater that is
22
23
24 127 acidified by magmatic gases uprising the magmatic chamber.
25

26 128 The weather in the region is typical of Andes, with precipitations over 2.000 mm/yr, mainly
27
28
29 129 snow, covering about 200 days/yr (from April to October). The temperatures are about 25°C on
30
31 130 summer and -14°C on winter, with an annual average of 7°C (Mas et al., 2000). There are not
32
33
34 131 isotopic data on precipitations at Copahue, either stable isotopes of water or tritium, as those
35
36 132 collected by the Global Network of Isotopes in Precipitation (GNIP) of the International Atomic
37
38
39 133 Energy Agency, in order to compare with values measured in water in this work or previous ones.
40
41 134 Tritium data are scarce and mainly from stations located close to Buenos Aires except for a few
42
43
44 135 data (n= 4) from the station of Cerro Ancasti at 1800m of altitude in the Andes, but 1016 km north
45
46 136 of Copahue. The tritium activity is 12.3 ± 1.6 Tritium units (TU) which is within the average for all
47
48 137 Argentina (n = 87) of 11.1 ± 3.3 TU (WISER database at [http://www-](http://www-naweb.iaea.org/napc/ih/IHS_resources_isohis.html)
49
50
51 138 [naweb.iaea.org/napc/ih/IHS_resources_isohis.html](http://www-naweb.iaea.org/napc/ih/IHS_resources_isohis.html)).

52
53 139

54 55 56 140 **3. METHODS**

57 58 141 *3.1 Sampling procedures*

59
60
61
62
63
64
65

1
2
3
4
5
6
7
8
9
10
11
12
13
14
15
16
17
18
19
20
21
22
23
24
25
26
27
28
29
30
31
32
33
34
35
36
37
38
39
40
41
42
43
44
45
46
47
48
49
50
51
52
53
54
55
56
57
58
59
60
61
62
63
64
65

142 Figure 1 shows locations of sampled hot springs and their association with the main surface
143 structural features of the Copahue geothermal area. Five hot spring water samples were collected
144 from the five thermal zones recognized at Copahue (AF, CB, LM, LMM, TC; Fig. 1). Four
145 geothermal exploration wells were drilled in the area (COP-1 to COP-4; Mas, 2005), but only one
146 (COP-2) is currently accessible for sampling and both the liquid phase (as steam condensate) and
147 the gas phase were collected.

148 Temperature, electric conductivity, and pH were measured *in situ*, and ionic balance
149 computation was carried out, based on the method described by Giggenbach and Gouguel (1989).
150 Water samples were filtered using a 0.45 µm filter (cellulose acetate) into precleaned, high density
151 polythene bottles (250 ml for cations, anions, and Sr isotopes; 500 ml for ³H and ¹⁴C) being careful
152 to avoid degassing or atmospheric CO₂ contamination for ¹⁴C analyses. Samples for cations and
153 trace element analyses were acidified with HNO₃ (Merck Suprapur[®]) 4N, 1 ml per 100 ml sample.
154 Samples for silica content determination were diluted at a ratio of 1:10 with milliQ water in order
155 to avoid silica precipitation. Water samples for stable isotopes of water were poured into 30 mL
156 HDPE bottles, filled to the top, and closed avoiding the trapping of air bubbles. Water and bubbling
157 gas for helium isotopes and for C and O isotopic analyses of CO₂ were collected in refrigeration-
158 type copper tubes sealed with clamps at both extremities, using armed PVC tubes connected to a
159 plastic funnel.

161 3.2 Analytical methods

162 Analyses of major anions and cations, and trace elements were performed at the Fluid
163 Geochemistry Laboratory of the Andean Geothermal Center of Excellence (CEGA), at University
164 of Chile, Santiago. Anion (F, Cl, and SO₄) concentrations were measured by ion chromatography
165 (Dionex[™] ICS-2100), while HCO₃ and CO₃ concentrations were determined by volumetric

1
2
3
4
5
6
7
8
9
10
11
12
13
14
15
16
17
18
19
20
21
22
23
24
25
26
27
28
29
30
31
32
33
34
35
36
37
38
39
40
41
42
43
44
45
46
47
48
49
50
51
52
53
54
55
56
57
58
59
60
61
62
63
64
65

titration. Cations concentrations (Na, K, Ca, Mg) were determined by atomic absorption spectrometry (Perkin Elmer, PinAAcle™ 900F). Trace elements concentrations were determined by inductively coupled plasma mass spectrometry (Thermo Scientific, iCAP Q ICP-MS). Silica contents were measured with spectrophotometry (Hanna Instruments HI 96705).

Stable isotopes of water ($\delta^2\text{H}$ and $\delta^{18}\text{O}$) and CO_2 ($\delta^{13}\text{C}$ and $\delta^{18}\text{O}$), strontium isotopic ratios ($^{87}\text{Sr}/^{86}\text{Sr}$), and helium isotopic ratios ($^3\text{He}/^4\text{He}$) were determined at GEOTOP, University of Quebec in Montreal.

A 0.2 ml volume of sample water was pipetted into a 3 ml vial, closed with a septum cap, and transferred to a 40°C heated rack. For $\delta^2\text{H}$, a hydrophobic platinum catalyst (Hokko beads) was added. After one hour, air in the vials was replaced with CO_2 (for $\delta^{18}\text{O}$) or H_2 (for $\delta^2\text{H}$) using the AquaPrep. Samples were left to equilibrate for 7 hours for $\delta^{18}\text{O}$ and 4 hours for $\delta^2\text{H}$. The equilibrated samples were analyzed with a Micromass model Isoprime isotope ratio mass spectrometer coupled to an AquaPrep system in dual inlet mode at the *Light stable isotope geochemistry laboratory* of the GEOTOP. Three internal reference waters were used to normalize the results on the V-SMOW-SLAP scale. A fourth reference water was analyzed as an unknown to assess the normalization. Results are given in delta units (δ) in ‰ vs VSMOW. The overall analytical uncertainty (1σ) is better than $\pm 0.1\text{‰}$ for $\delta^{18}\text{O}$ and $\pm 2.0\text{‰}$ for $\delta^2\text{H}$.

The CO_2 was separated from residual humidity in the copper tube, if any, using an isopropyl dry ice mix trap, and a liquid nitrogen trap was used to separate CO_2 from other incondensable gases, following procedures described in Richard et al. (2019). Because the amount of residual water is negligible, even at ambient temperature the exchange of ^{18}O between water and CO_2 will not affect the $\delta^{18}\text{O}\text{-CO}_2$ (Richard et al., 2019). Indeed Figure 3 shows that $\text{CO}_2\text{-H}_2\text{O}$ re-equilibration occur *in situ* at geothermal pool temperatures of 90-100°C. After recovering a variable

1
2
3
4
5
6
7
8
9
10
11
12
13
14
15
16
17
18
19
20
21
22
23
24
25
26
27
28
29
30
31
32
33
34
35
36
37
38
39
40
41
42
43
44
45
46
47
48
49
50
51
52
53
54
55
56
57
58
59
60
61
62
63
64
65

189 amount of CO₂ gas in a Pyrex glass vessel, the isotopic compositions of C and O were determined
190 using an Isoprime 100 Dual Inlet Isotope Ratio Mass Spectrometer (DI-IRMS) at the *Light stable*
191 *isotope geochemistry laboratory* of the GEOTOP (Richard et al., 2019). The samples were
192 compared to a working CO₂ standard that had been normalized to the V-PDB scale.

193 Strontium isotopic ratios (⁸⁷Sr/⁸⁶Sr) were analyzed in water samples and the liquid
194 condensate of COP-2 well by thermal ionization mass spectrometry (TIMS Triton plus) at the
195 *Radiogenic and non-traditional stable isotope geochemistry laboratory* of GEOTOP. This
196 technique requires the chemical separation of Sr, which was carried out by evaporating the water
197 sample on a hot plate, and then uptaking the salt in 3 mol/L HNO₃. The obtained solution was
198 centrifuged and purified onto a Sr-spec ion exchange column to extract the Sr in HNO₃ 3N/0.05N
199 high purity reagents. The solution is then pipetted on a filament to be analyzed by TIMS. The
200 NBS987 standard (100ng) was measured at 0.71026±0.00002 at the beginning of the analytical
201 session, obviously on a separate filament and thus eliminating any “memory” effect on samples.

202 The isotopic ratios of He (³He/⁴He) were measured using a noble gas mass spectrometer at
203 the *Montreal Noble Gas Laboratory (GRAM)* of GEOTOP. The gas mixture in the copper tubes
204 was diluted manually in a specific volume until pressure, measured on a Baratron Gauge, was less
205 than 10 mbar. The reactive gases were removed using one Ti-getter at 600 °C for 15 min followed
206 by 10 min at ambient temperature and two SAES ST-707 getters at 100 °C for 15 min followed by
207 10 min at ambient temperature. Gases were then adsorbed onto an Advanced Research System
208 (ARS[®]) cryogenic trap containing activated charcoal at 10K and released sequentially at 35K (He)
209 and 110K (Ne). He and Ne isotopes were measured on a Thermo[®] HELIX-MC using the axial
210 Faraday detector by peak jumping, except for ³He, which was measured by ion counting on the
211 axial Compact Discrete Dynode[™] (CDD) detector. Blanks are typically on the order of 0.01% for
212 He and Ne. Obtained signals were calibrated against a known aliquot of standard air. Typical

1
2
3
4 213 standard reproducibility for ^4He and ^{20}Ne are 1.5–2%. Errors on the $^3\text{He}/^4\text{He}$ ratios are about 2%
5
6
7 214 at 1σ .

8
9 215 Assuming that the Air Saturated Water (ASW) neon content is significantly higher than in
10
11 216 mantle and crustal gases, the measured $^3\text{He}/^4\text{He}$ ratio, normalized to that of the atmosphere $R_a =$
12
13
14 217 1.384×10^{-6} or R/R_a can be corrected for the presence of atmospheric helium (R_c/R_a) using the
15
16 218 $^4\text{He}/^{20}\text{Ne}$ ratio of the sample (Craig et al., 1978):

$$R_c/R_a = [R/R_a - r]/(1 - r), \quad (1)$$

17
18
19 219 where “r” is defined as:

$$r = ({}^4\text{He}/{}^{20}\text{Ne})_{\text{ATM}} / ({}^4\text{He}/{}^{20}\text{Ne})_{\text{obs}}, \quad (2)$$

20
21 220
22
23
24 221
25
26 222
27
28
29 223 where $({}^4\text{He}/{}^{20}\text{Ne})_{\text{ATM}}$ and $({}^4\text{He}/{}^{20}\text{Ne})_{\text{obs}}$ are the atmospheric and measured ${}^4\text{He}/{}^{20}\text{Ne}$ ratios
30
31 224 respectively. If air is accidentally added during sampling the $({}^4\text{He}/{}^{20}\text{Ne})_{\text{ATM}}$ is equal to that of the
32
33
34 225 atmosphere ($({}^4\text{He}/{}^{20}\text{Ne})_{\text{Air}} = 0.3185$), while if it assumed that atmospheric He and Ne derive from
35
36 226 the meteoric water endmember it should be calculated at the ASW conditions of temperature
37
38
39 227 (MAAT or Mean Annual Average Temperature) which in Copahue is 11°C ($({}^4\text{He}/{}^{20}\text{Ne})_{\text{ASW}} = 0.274$;
40
41 228 solubility data of Smith and Kennedy, 1983). For sake of consistency with previous results from
42
43
44 229 the same area (e.g., Augusto et al., 2013; Tassi et al., 2017), the $({}^4\text{He}/{}^{20}\text{Ne})_{\text{Air}} = 0.3185$ was retained
45
46 230 as value for air correction.

47
48 231 Radiocarbon (^{14}C) was determined for the dissolved inorganic carbon (DIC) fraction on a
49
50
51 232 3MV accelerator mass spectrometer (AMS) at the University of Ottawa. The $^{12,13,14}\text{C}^{+3}$ ions were
52
53 233 measured at 2.5 MV terminal voltage with Ar stripping (Crann et al., 2017). Radiocarbon contents
54
55
56 234 are reported as modern carbon fraction ($F^{14}\text{C}$), according to Reimer et al. (2004), calculated using
57
58 235 the $^{14}\text{C}/^{12}\text{C}$ ratios of the sample and the oxalic acid standard. All values were corrected and

1
2
3
4 236 normalized using the $\delta^{13}\text{C}$ ratios and the same standard; the calculations are shown in Reimer et al.
5
6
7 237 (2004). Calibration was performed using OxCal 4.2.4 software. Finally, the ages were calculated
8
9 238 using the formula (Stuiver and Polach, 1977):

$$^{14}\text{C years BP} = -8033 \ln (F^{14}\text{C}) \quad (3),$$

10
11 239
12
13
14 240
15
16 241
17
18
19 242 where BP stands for “Before Present” and corresponds to the year 1950.

20
21 243 Tritium concentrations were analyzed at the Environmental Isotope Laboratory (EIL) at the
22
23
24 244 University of Waterloo, Canada. Liquid Scintillation Counting (LSC) was used for tritium analyses.
25
26 245 The samples were concentrated 15 times by electrolysis prior to performing the count. The
27
28
29 246 detection limit for the enriched samples is 0.8 TU (Heemskerk and Johnson, 1998).
30

31 32 247 **4. RESULTS AND DISCUSSION**

33
34 248 Table 1 reports the concentrations of major ions and trace elements measured in the water
35
36
37 249 samples from the five hot springs, and one steam condensate from the geothermal well. Table 2
38
39 250 reports the stable isotopic composition of water, CO_2 , the $^{87}\text{Sr}/^{86}\text{Sr}$ ratios, the $^3\text{He}/^4\text{He}$ ratio (R/Ra),
40
41
42 251 the $^4\text{He}/^{20}\text{Ne}$ ratio, and the air-corrected Rc/Ra. Finally, the ^{14}C activity (as a fraction of present-
43
44 252 day activity or 120 pMc) and that of ^3H (TU) are also reported in Table 2.
45
46

47 253 *4.1 Water chemical composition*

48
49 254 The temperatures of sampled waters ranged from 55.4 °C to 93.5 °C. Well COP-2 presented
50
51
52 255 a vapor temperature of 220°C. The condensate from COP-2 should have a temperature of 92°C,
53
54 256 corresponding to the water boiling point at the well-head elevation of approximately 2075 m.a.s.l.
55
56 257 Hot spring samples LMM, LM, AF, and CB show highly acidic pH (1.9 to 2.4), and their chemical
57
58
59 258
60
61
62
63
64
65

1
2
3
4 259 compositions are dominated by SO_4 (496 to 6515 mg/L) as the principal anion, classifying them as
5
6
7 260 steam-heated acid-sulfate waters (Giggenbach and Stewart, 1982). Hot spring sample TC shows a
8
9 261 neutral pH of 6.8, with HCO_3 as the dominant chemical species. The HCO_3 in geothermal waters
10
11 262 could be produced by the reaction of CO_2 with Na-K silicates, by the dissolution of carbonates, or
12
13
14 263 by the direct dissolution of CO_2 in water, especially where there are high fluxes of this gas (Fournier
15
16 264 and Truesdell, 1970; Gizaw, 1996). Previous studies carried out in the Copahue area showed
17
18
19 265 significant CO_2 fluxes (average value of $112.25 \text{ g m}^{-2}\text{d}^{-1}$; Roulleau et al., 2017) from soil gases,
20
21 266 which are related to local tectonic structures (Chiodini et al. 2015; Roulleau et al., 2017; Lamberti
22
23
24 267 et al., 2019). The chemical composition of sample TC may be derived from the interaction of
25
26 268 surface waters with a high- CO_2 concentration steam, relative to acid gas species, such as H_2S , HCl
27
28
29 269 and HF .

30
31 270 Sample COP-2 corresponds to the condensed steam from COP-2 well, which reaches the
32
33 271 vapor-dominated geothermal reservoir at 1400 m b.g.l (Sierra et al., 1992; Panarello, 2002). The
34
35
36 272 alkaline pH (8.5) and the predominance of dissolved HCO_3 (33.3 mg/L) likely corresponds to CO_2
37
38 273 dissolution, while the much lower concentrations of Cl (0.9 mg/L) and SO_4 (0.81 mg/L) are likely
39
40
41 274 due to the dissolution of HCl and H_2S . Therefore, these results show that CO_2 is the dominant gas
42
43 275 in the dry steam phase at depth, in accordance with the gas composition, which shows a CO_2
44
45 276 concentration of 870 to 989 mmol/mol, significantly higher than the concentration of H_2S (2.5 -
46
47
48 277 150 mmol/mol) (Agusto et al., 2013; Roulleau et al., 2016).

49
50 278 Trace elements present a wide range of concentrations, varying from a few $\mu\text{g/L}$ to hundreds
51
52
53 279 of mg/L. Iron and Al are the most abundant elements, presenting concentrations ranging from 27.9
54
55 280 $\mu\text{g/L}$ to 253 mg/L and 26.8 $\mu\text{g/L}$ to 756 mg/L respectively. Manganese and B present concentrations
56
57
58 281 varying from 10.5 $\mu\text{g/L}$ to 3.5 mg/L and 1.4 $\mu\text{g/L}$ to 5.5 mg/L respectively. Concentrations of Li,
59
60
61

1
2
3
4 282 Rb, Sr, Ba, Cs, As, Cr, and Ni are in lower, ranging from fractions to hundreds of $\mu\text{g/L}$ (Table 1).
5

6
7 283 Figure 2a-f shows trace elements plotted versus the SO_4 contents measured in the hot spring
8
9 284 samples and the well condensate. The positive correspondence between SO_4 and Al, Fe, Mn, Rb,
10
11 285 As, and Cs supports the hypothesis of a progressive isochemical dissolution of the host rocks due
12
13
14 286 to the acidic and immature nature of the waters (Stefánsson and Arnórsson, 2005). Silica contents
15
16 287 of the hot spring samples vary from 54.25 (LM) to 369 (LMM) mg/L , and, consistent with the trace
17
18
19 288 element data, the highest concentrations are related to samples CB, LMM, and AF, suggesting that
20
21 289 the SiO_2 origin is dominated by rock dissolution at the surface.
22
23

24 290 25 26 291 *4.2. Stable isotope composition of sampled waters and gas phases* 27

28
29 292 The $\delta^{13}\text{C-CO}_2$ values for the hot spring samples and COP-2 (Table 2) range between -7.81
30
31 293 ‰ and -7.23 ‰ versus V-PDB, typical of magmatic CO_2 ($-6\pm 2\%$; Javoy et al., 1986) and similar
32
33
34 294 to values measured by Agosto et al. (2013) in the same areas. $\delta^{18}\text{O-CO}_2$ ranges between -3.31 and
35
36 295 +5.45‰ versus V-PDB. In hydrothermal system, variations in $\delta^{18}\text{O-CO}_2$ are expected to be
37
38
39 296 controlled by the ^{18}O exchange between steam and CO_2 (Chiodini et al., 2000), the extent of
40
41 297 which depends on the temperature at which this exchange proceeds and the initial ^{18}O
42
43
44 298 composition of H_2O and CO_2 . In Figure 3, the fractionation factor “ α ” between CO_2 and H_2O of
45
46 299 ^{18}O is reported versus the inverse of the measured temperature at the hot spring or in the well.
47
48
49 300 The isotopic equilibrium between H_2O and CO_2 is represented by the “per mil fractionation” or
50
51 301 “ $1000\ln\alpha$ ”, which is calculated as follows (Chiodini et al., 2000):
52

$$53 302
54
55
56 303 \quad 1000 \ln \alpha_{\text{CO}_2\text{-H}_2\text{O}} = [(1000 + \delta^{18}\text{O}_{\text{CO}_2}) / [(1000 + \delta^{18}\text{O}_{\text{CO}_2})] \quad (4)
57$$

1
2
3
4 305 The three curves reported in Fig. 3 represent the variation in $1000 \ln \alpha_{CO_2-H_2O}$ with
5
6
7 306 temperature, as calculated by Friedman and O'Neil (1977), Richet et al. (1977), and the
8
9 307 experimental curve of Chiodini et al. (2000). The sampled waters show $\delta^{18}O$ -CO₂ in equilibrium
10
11
12 308 with the ¹⁸O of water, except for the condensate, COP-2, which shows a higher $1000 \ln \alpha_{CO_2-H_2O}$
13
14 309 value, perhaps indicative of incomplete re-equilibration, as observed in other geothermal wells in
15
16
17 310 Larderello (Panichi et al., 1977) and in Mexico (Richard et al., 2019).

19 311 The results showed in Fig. 3 indicate that a re-equilibration took place between the CO₂
20
21
22 312 and the H₂O in our samples and thus the oxygen isotopic composition of water needs to be
23
24 313 corrected of such a re-equilibration. The $\delta^{18}O$ of H₂O corrected for the exchange with the CO₂ or
25
26
27 314 $\delta^{18}O_{H_2O}^f$ can be calculated following the equation (Karolyt  et al., 2017):
28
29
30 315

$$\delta^{18}O_{H_2O}^f = (\delta^{18}O_{CO_2}^i - 1000 \ln \alpha) \times X_{CO_2} + \delta^{18}O_{H_2O}^i \times (1 - X_{CO_2}) \quad (5),$$

32 316
33
34
35 317
36
37 318 where X_{CO_2} is the fraction of oxygen in the system sourced from the CO₂. Based on steam/gas ratios
38
39
40 319 and CO₂ molar contents in the geothermal surface pools sampled by Agosto et al. (2013), the X_{CO_2}
41
42 320 was estimated to vary between 0.026 to 0.037. Correction is practically nil for samples LM, AF
43
44
45 321 and COP-2, while the isotopic shift in the $\delta^{18}O_{H_2O}^f$ range from 0.11‰ for sample Tc and 0.55‰
46
47 322 for samples CB and LMM (Table 2).
48
49

50 323 Figure 4 shows the δ^2H versus $\delta^{18}O$ diagram of the sampled waters and the condensate of
51
52 324 COP2 well, together with the local meteoric water line (LMWL), as calculated by local rainfall
53
54
55 325 data from Agosto and Varekamp (2016). The term “EVAP” refers to the evaporation line which
56
57 326 shows the effects of evaporation of pure meteoric waters at mean ambient temperatures (about 11
58
59
60 327 °C) and local relative humidity (60 %). This was calculated by Agosto and Varekamp (2016) to
61
62
63
64
65

1
2
3
4 328 explain the stable isotopic composition of evaporated surface waters from streams, some
5
6 329 geothermal pools and the crater lake.

7
8
9 330 The measured $\delta^2\text{H}$ and the CO_2 -corrected $\delta^{18}\text{O}$ correlates and the calculated straight line
10
11 331 passes through the meteoric water endmember defined by Panarello (2002) of $\delta^2\text{H}$ of -80‰ and a
12
13 332 $\delta^{18}\text{O}$ -11‰ and an andesitic water source, as defined by Taran and Zelenski (2015). The straight
14
15 333 line has a lower slope than the evaporation line, and equal to $\delta^2\text{H} = 3.2 \times \delta^{18}\text{O} - 45.2$, which is
16
17 334 compatible, within the 95% confidence interval, with that calculated by Augusto and Varekamp
18
19 335 (2016), of $\delta^2\text{H} = 3.6 \times \delta^{18}\text{O} - 41.65$ for the fluids that define the local Copahue volcano-
20
21 336 hydrothermal system. The $\delta^{18}\text{O}$ does not show any pronounced horizontal shift toward higher
22
23 337 values, which could indicate little water-rock interaction processes within the hydrothermal system,
24
25 338 as suggested by Augusto et al. (2013).
26
27
28
29
30
31

32 339 33 34 340 *4.3 $^{87}\text{Sr}/^{86}\text{Sr}$ isotope ratios: sources and water/rock interaction effects*

35
36 341 Strontium isotopic ratios ($^{87}\text{Sr}/^{86}\text{Sr}$) of sampled hot springs and well condensate COP-2 are
37
38 342 listed in Table 2. The measured $^{87}\text{Sr}/^{86}\text{Sr}$ ratios cover a narrow range between 0.70396 ± 0.00006
39
40 343 (AF) to 0.70452 ± 0.00013 (LM) with except the COP-2 condensate which shows a more radiogenic
41
42 344 value of 0.70697 ± 0.00039 (Table 2). The distribution of strontium between water and rocks is
43
44 345 mainly determined by dissolution or by equilibrium isotope exchange between the rock and the
45
46 346 fluid and $^{87}\text{Sr}/^{86}\text{Sr}$ generally reflect those of the host rock (Notsu et al., 1991).
47
48
49
50

51 347 In Figure 5, $^{87}\text{Sr}/^{86}\text{Sr}$ ratios are plotted against the temperature of the sampled geothermal
52
53 348 water (a), the SiO_2 contents (b) and the $\delta^{13}\text{C}\text{-CO}_2$ (c). The orange area in Figs. 5a-c delineates the
54
55 349 range of strontium isotopic signatures of the rock units composing the CCVC. These are
56
57 350 trachyandesites to rhyolites from the Riscos Bayos ignimbrite, the 2000 eruption of Copahue and
58
59
60
61
62
63
64
65

1
2
3
4
5
6
7
8
9
10
11
12
13
14
15
16
17
18
19
20
21
22
23
24
25
26
27
28
29
30
31
32
33
34
35
36
37
38
39
40
41
42
43
44
45
46
47
48
49
50
51
52
53
54
55
56
57
58
59
60
61
62
63
64
65

351 the caldera wallrock from Caviahué measured by Varekamp et al. (2006) ($^{87}\text{Sr}/^{86}\text{Sr}$ from
352 0.70376±0.00002 to 0.70399±0.00002); volcanic sequences of the Cola de Zorro (Hualcupén) Fm.
353 with a $^{87}\text{Sr}/^{86}\text{Sr}$ ratio of 0.70393±0.00003 (Rouilleau et al., 2018); the ignimbrites of Las Mellizas
354 ($^{87}\text{Sr}/^{86}\text{Sr}$ = 0.70387±0.00003; Rouilleau et al., 2018); and the Copahué volcanic series ($^{87}\text{Sr}/^{86}\text{Sr}$ =
355 0.70389±0.00007 to 0.70405±0.00002; Rouilleau et al., 2018), including recent lavas erupted by
356 the Copahué volcano. These $^{87}\text{Sr}/^{86}\text{Sr}$ values are higher than those expected for a back-arc basaltic
357 source (0.70330; Varekamp et al., 2006) and it has been explained by local contamination of the
358 magma source with material from the subducting Nazca plate sediments (Pacific Ocean detrital
359 sediments in Varekamp et al., 2006).

360 The $^{87}\text{Sr}/^{86}\text{Sr}$ values reported for LMM, CB, and AF are within the range of values measured
361 in the volcanic rocks composing the CCVC (Figs. 5a-c) whereas samples TC, LM, and COP-2
362 present higher $^{87}\text{Sr}/^{86}\text{Sr}$ values, suggesting mixing with a fluid with higher radiogenic $^{87}\text{Sr}/^{86}\text{Sr}$ and
363 which could be the endmember composition measured in COP-2. Sample COP-2 shows the highest
364 radiogenic $^{87}\text{Sr}/^{86}\text{Sr}$ ratio of 0.70697, but the lowest SiO₂ concentration (Fig. 5b), which could
365 appear strange at first sight. However, COP-2 represents the steam condensate from the steam cap
366 lying above the geothermal reservoir, at a depth of ~1000 m (Barcelona et al., 2019), resulting
367 from the boiling of reservoir water at depth. Thus, it is normal that SiO₂ has partitioned mostly in
368 the liquid phase at depth and that the condensate is deprived of silica, but still conserves the original
369 $^{87}\text{Sr}/^{86}\text{Sr}$ ratio.

370 The $^{87}\text{Sr}/^{86}\text{Sr}$ ratio measured in COP-2 condensate is anomalously high compared the other
371 measured values (Table 2). High $^{87}\text{Sr}/^{86}\text{Sr}$ ratios are not found in volcanic rocks of this area but are
372 common for the northern Southern volcanic zone (Varekamp et al., 2006), which is strongly
373 affected by contributions from the subducting Nazca plate sediments. The radiogenic $^{87}\text{Sr}/^{86}\text{Sr}$

1
2
3
4 374 value measured in COP-2 has likely a local source and could be inherited either 1) from depth-
5
6 375 seated granitoids or 2) from the Neuquén marine sequence, located 2 km below sea level under the
7
8
9 376 Copahue-Caviahue volcanic sequence (Varekamp et al., 2006). At depths of 1000 m below ground
10
11 377 level, at the bottom of the drill cores, the presence of a porphyritic intrusive body has been
12
13
14 378 recognized (JICA, 1992). The fluid-rock interaction with such an intrusive unit may have shifted
15
16 379 the $^{87}\text{Sr}/^{86}\text{Sr}$ ratios of fluids toward more radiogenic signatures than those characteristics of fluids
17
18
19 380 having interacted with the Plio-Quaternary volcanic sequences of the CCVC. Porphyry generally
20
21 381 show high $^{87}\text{Sr}/^{86}\text{Sr}$ ratios, with values of up to 0.7050-0.7080 (e.g., Thorpe et al., 1981; Maydagan
22
23
24 382 et al., 2016). Varekamp et al. (2006) suggested the contribution of local sediments from the Nequém
25
26 383 basin marine sequence to explain, i.e. the $\delta^{13}\text{C}\text{-CO}_2$ measured in the geothermal gases which are
27
28
29 384 up to -8‰ vs V-PDB. Though the $\delta^{13}\text{C}\text{-CO}_2$ value is within the range expected for mantle carbon
30
31 385 ($\delta^{13}\text{C} = -6 \pm 2\text{‰}$; Javoy et al., 1986) particularly in volcanic arcs (Mason et al., 2017), Varekamp et
32
33
34 386 al. (2006) suggested that isotopically lighter carbon from organic-rich sediments could have
35
36 387 contributed to the CO_2 of the CCVC gaseous manifestations. It is interesting to note in Fig. 5c, that
37
38
39 388 the $^{87}\text{Sr}/^{86}\text{Sr}$ ratio vs the $\delta^{13}\text{C}\text{-CO}_2$ suggests a mixing between two fluids with different C and Sr
40
41 389 isotopic composition (the mixing should be a hyperbola as represented in Fig. 5c). The fluid
42
43
44 390 represented by the condensate of COP-2 is more enriched in radiogenic Sr and in isotopically
45
46 391 lighter C, suggesting possible crustal Sr and C addition to the mixture.
47
48
49 392

50 51 393 *4.4 $^3\text{He}/^4\text{He}$ isotope ratios: meteoric, crustal and mantle contributions*

52
53 394 The helium isotopic ratio (R/Ra) of the hot springs and well COP-2 vary between 4.6Ra
54
55
56 395 (AF) and 8.28Ra (LMM) (Table 2; Fig. 6), and values are consistent with those measured in
57
58
59 396 previous studies (Agusto et al., 2013; Roulleau et al., 2016; 2018; Tassi et al., 2017). Overall, R/Ra
60
61
62
63
64
65

1
2
3
4
5
6
7
8
9
10
11
12
13
14
15
16
17
18
19
20
21
22
23
24
25
26
27
28
29
30
31
32
33
34
35
36
37
38
39
40
41
42
43
44
45
46
47
48
49
50
51
52
53
54
55
56
57
58
59
60
61
62
63
64
65

397 values of the Copahue fluids are significantly higher than the atmospheric value ($R/Ra = 1.0$) and
398 the crustal value ($R/Ra = \sim 0.02Ra$; Morrison and Pine, 1955), indicating a dominant mantle He
399 contribution ($R/Ra = 8.0 \pm 1$; Allègre et al., 1995; Fig. 6), diluted locally by the addition of
400 radiogenic and/or atmospheric 4He .

401 The mixing hyperbolas plotted in Fig. 6 suggest that the He isotopic composition of LM,
402 LMM, CB, and TC waters results from mixing between 1) deep-seated fluids containing mantle
403 He with R/Ra values between 7 Ra and 9 Ra and either 2) air ($R/Ra = 1$ and $^4He/^{20}Ne = 0.3185$) or
404 3) meteoric water containing dissolved atmospheric He at ASW conditions. In the case of Copahue
405 geothermal field, recharge has been identified to be in Chanco-có and Anfiteatro areas, in addition
406 to the water recharge occurring on the flank of the Copahue volcano (Agusto et al., 2013). The
407 Mean Annual Air Temperature (MAAT) in this area is $11^\circ C$ (Agusto and Varekamp, 2016) leading
408 to a $^4He/^{20}Ne$ ratio in the meteoric water at the recharge of 0.274 (using solubility data from Smith
409 and Kennedy, 1983).

410 Samples COP-2 and AF pass through a hyperbola curve that suggests mixing between either
411 air or meteoric water and geothermal waters having accumulated some radiogenic 4He , with
412 resulting lower R/Ra values of the second endmember of 6.5 and 4.0, respectively. The contribution
413 of radiogenic (crustal) helium to the mixture can be determined using ternary mixing equations
414 (Pinti et al., 2019):

$$R/Ra_{obs} = R/Ra_{mtl} * M + R/Ra_{crust} * C + R/Ra_{ASW} * A \quad (6)$$

$$1/(^4He/^{20}Ne)_{obs} = M/(^4He/^{20}Ne)_{mtl} + C/(^4He/^{20}Ne)_{crust} + A/(^4He/^{20}Ne)_{ASW} \quad (7)$$

$$M + C + A = 1 \quad (8),$$

1
2
3
4 420 where the subscripts obs, mtl, crust, and ASW refer to the observed sample, the mantle end-
5
6
7 421 member, the crustal end-member, and the freshwater end-member respectively and M, C, and A are
8
9 422 the proportions of the three above-listed components. The radiogenic helium fraction is 19.6% of
10
11 423 the total helium in the COP-2 condensate, and up to 42.1% in sample AF. The other parameter that
12
13
14 424 seems to be related to water-rock interaction, namely the $^{87}\text{Sr}/^{86}\text{Sr}$ ratio, does not show a clear
15
16 425 relationship with the helium isotopic composition of water, particularly for these two samples
17
18
19 426 (COP-2 and AF). This could be due to different fluid ascent pathways through the field, with COP-
20
21 427 2 and AF exchanging radiogenic ^{87}Sr with different reservoir and/or basement rocks.

22
23
24 428

25
26 429 *4.5 ^3H and ^{14}C data: water residence time*

27
28
29 430 The activities of both ^3H and ^{14}C were measured in well condensate COP-2 and in the hot
30
31 431 springs LM, LMM, CB, TC, and AF (Table 2). The ^{14}C should provide a direct measure of water
32
33 432 residence times in the range of 1 to 40 ka, whereas the abundance of ^3H reflects recharge processes
34
35
36 433 since the atomic bomb test period in the 1950s and early 1960s (Birkle et al., 2001; Aggarwal,
37
38 434 2013). Unfortunately, there have been few attempts to use these two water chronometers in
39
40
41 435 geothermal systems (e.g., Le Goff and McMurtry, 2000; Birkle et al., 2016; Morata et al., 2019)
42
43 436 because geothermal waters often have residence times beyond the limit of the ^3H method (Goff &
44
45
46 437 Janik, 2000), and only shallow hydrothermal circuits can be dated using this method, such as, for
47
48 438 example, Beppu in Japan (Kitaoka, 1990) and Poás Volcano in Costa Rica (Rowe et al., 1995).
49
50
51 439 Furthermore, the dominant volatile species in geothermal reservoirs is often volcanic CO_2 , which
52
53 440 constitutes an infinite pool of dead carbon masking the cosmogenic ^{14}C activity (e.g., Birkle et al.,
54
55 441 2016).

56
57
58 442 The ^{14}C activity was measured in three of the six samples, with very little activity fraction
59
60 443 values, of 0.113 ± 0.0013 (LM), 0.1651 ± 0.0014 (COP-2), and 0.1853 ± 0.0018 (TC) (Table 2). The

1
2
3
4 444 ^{14}C calculated ages yield values of $13,540\pm 80$ yrs BP for sample TC, $14,470\pm 69$ yrs BP for sample
5
6 445 COP-2, and $17,520\pm 93$ yrs BP for sample LM (Table 2). Samples LMM, AF, and CB, where
7
8
9 446 radiocarbon was not detected, presented a dissolved organic carbon (DOC) content 10 to 25 times
10
11 447 higher than the DIC (Table 2).

12
13
14 448 Very low tritium activity of 0.8 TU, close to the detection limit of the method, was
15
16 449 determined only in two samples, LMM and CB (Table 2). This suggests that waters have residence
17
18
19 450 times older than 70 yrs, although a precise age cannot be estimated. This result is important because
20
21 451 the general interpretation on the origin of the geothermal pools on the Copahue volcano flanks is
22
23
24 452 steam-heated glacial meltwater infiltrating the summit crater (at ~ 3000 m.a.s.l.) and emerging at
25
26 453 lower altitudes of 1600 m.a.s.l. It would expect that these waters have very short residence times,
27
28
29 454 while both ^3H and ^{14}C data suggest the contrary. This could imply either 1) that the infiltrating
30
31 455 meteoric water flow through a more complex and deeper hydrogeological circuit or 2) that they are
32
33 456 mixed with an older water component.

34
35
36 457 Figure 7a shows the $\delta^2\text{H}$ of water versus the $^4\text{He}/^{20}\text{Ne}$ ratio. This latter ratio can indicate
37
38
39 458 the degree of air contamination of a noble gas water sample or represent the ratio of atmospheric
40
41 459 ^4He and ^{20}Ne dissolved in the meteoric water at the recharge (ASW conditions). Except for samples
42
43 460 CB and LMM, the $^4\text{He}/^{20}\text{Ne}$ ratio correlated with the $\delta^2\text{H}$ value of water. This supports the
44
45
46 461 hypothesis that $^4\text{He}/^{20}\text{Ne}$ variability indicates the mixing between meteoric water showing ASW-
47
48 462 like $^4\text{He}/^{20}\text{Ne}$ ratios, and geothermal water, showing a heavier, “andesitic”, $\delta^2\text{H}$ composition and a
49
50
51 463 higher $^4\text{He}/^{20}\text{Ne}$ ratio due to addition of terrigenic ^4He . This result does not agree with the general
52
53
54 464 interpretation of the Copahue geothermal pools being steam-heated meteoric waters. If it is the
55
56 465 case, we should not see any correlation between $^4\text{He}/^{20}\text{Ne}$ – transported by the steam phase – and
57
58 466 the stable isotopic composition of the hydrogen in the water phase. This can be the case of samples
59
60
61
62
63
64
65

1
2
3
4 467 CB and LMM which indeed do not follow this general trend. From the $\delta^2\text{H}$ values of the two
5
6
7 468 possible endmembers ($\delta^2\text{H} = -80\text{‰}$ for meteoric water; Augusto and Varekamp, 2016; $\delta^2\text{H} = -20\text{‰}$
8
9 469 for the andesitic water; Giggenbach, 1992) and using a simple binary mixing equation, the fraction
10
11
12 470 of “andesitic water” in sample AF is practically nil but increase up to 51% in sample LM.

13
14 471 Figure 7b shows the $^4\text{He}/^{20}\text{Ne}$ ratios versus the DOC/DIC ratios. The ^{14}C and minimum ^3H
15
16 472 ages are reported for the corresponding samples. The trendline in Fig.7b, showing a relationship
17
18
19 473 between the $^4\text{He}/^{20}\text{Ne}$ and the ratio between DOC and DIC, confirms the hypothesis of progressive
20
21
22 474 mixing between surface groundwaters, where the dominant C source is organic matter, and deep
23
24 475 geothermal waters, where the main C source is likely volcanic CO_2 and possibly C from carbonate
25
26 476 dissolution. It is worth noting that the ages and temperatures of the waters decrease from $17,520 \pm 93$
27
28
29 477 BP and 93°C to ≥ 70 yrs and 65°C along the trendline, further supporting this hypothesis.

30 31 478 32 33 34 479 *4.6. Fluid circulation model at Copahue*

35
36 480 By combining the structural information available for the study area with isotopic data from
37
38
39 481 this study and from Roulleau et al. (2016), a conceptual model of fluid circulation in the CCVC is
40
41 482 presented in Fig. 8.

42
43 483 The recent study of Lundgren et al. (2017), combining InSAR and seismic data collected
44
45
46 484 during the 2011-2016 period of unrest, proposes the presence of two magma sources beneath
47
48 485 Copahue volcano, with different degrees of magma differentiation (Cannatelli et al., 2016). The
49
50
51 486 shallow source is located 2.5 km beneath the surface and is centered under the volcanic edifice.
52
53 487 The second source is deeper, located 7-10 km below the surface and extending northeast, under the
54
55
56 488 center of the Caviahue caldera (Fig. 8).

57
58 489 The CCVC fluid composition is essentially dominated by the mixing between two
59
60
61

1
2
3
4 490 components: the deep seated magmatic/hydrothermal fluids and the shallow groundwater system.
5
6
7 491 The deep-seated fluids are degassing from the two magmatic sources identified below the
8
9 492 volcanic/hydrothermal system. Helium isotopes provide a reliable tool to separate the two members
10
11 493 of the deep signal, whereas the water chemical composition and the other isotopes presented in this
12
13
14 494 study provide the opportunity to disentangle the deep signal from the shallow groundwater input.
15
16 495 The main structures in the Caviahué caldera are NE-striking normal faults, resulting in a horst-and-
17
18
19 496 graben setting, and NW-striking strike-slip faults, interpreted as accommodation zones between the
20
21 497 main extensional structures (Lamberti et al., 2019). These sets of faults control the hydrothermal
22
23
24 498 activity and CO₂ degassing in the CCVC (Chiodini et al., 2015; Roulleau et al., 2017; Lamberti et
25
26 499 al., 2019). The TC, LM, LMM, and CB hydrothermal areas show helium ratios of up to 8.35Ra and
27
28
29 500 higher CO₂ flux than AF and CC (Chiodini et al., 2015; Roulleau et al., 2016, 2017; Lamberti et
30
31 501 al., 2019). These characteristics suggest independent fluid pathways and sources for AF-CC and
32
33
34 502 TC-LM-LMM-CB hydrothermal areas (Barcelona et al., 2020). The hydrothermal zones of LM,
35
36 503 LMM, CB, and TC are spatially associated with damage zones, related to the interaction of main
37
38 504 deep-rooted NE-SW and NW-SE normal faults (Fig. 8), presenting a high density of fractures, high
39
40
41 505 dilatational tendency, and high vertical permeability (Melnick et al., 2006; Lamberti et al., 2019;
42
43 506 Barcelona et al., 2020). These faults generate a preferential zone, which allows the ascent of
44
45
46 507 hydrothermal fluids from the deeper magmatic reservoir to the surface. The thermal springs LMM
47
48 508 and CB, lie on the same NW-SE normal fault (Figure 8), despite showing mantle-derived helium
49
50
51 509 isotopes and stable water isotopes of magmatic origin, present evidence of mixing with meteoric
52
53 510 water at the surface, perhaps due to local variation in the thickness of the groundwater aquifer, with
54
55 511 which the hydrothermal fluids interact during their ascent to the surface. Both LMM and CB
56
57
58 512 samples present the highest concentration of silica and the tritium activity indicates water residence
59
60 513 time >70 years, which represents the minimum age for the meteoric recharge. It suggests that,

1
2
3
4 514 nevertheless the water composition is affected by a significant meteoric water component, the water
5
6 515 circulation patterns are more complex and deeper than previously proposed.

7
8
9 516 The AF and CC hydrothermal zones, located closer to the volcanic edifice, are spatially
10
11 517 associated with shallower sets of NE-SW- and NW-SE-oriented normal faults respectively
12
13 518 (Melnick et al., 2006; Lamberti et al., 2019; Barcelona et al., 2020). These shallower sets of faults
14
15 519 likely represent the escape route for the hydrothermal fluids exsolved from the shallow magmatic
16
17 520 reservoir (Lundgren et al., 2017), presenting a lower $^3\text{He}/^4\text{He}$ ratio. The hydrothermal fluids
18
19 521 separated from more evolved magmas, stored at shallow depths, present lower helium ratios due
20
21 522 magma chamber degassing of the original mantle component combined with radiogenic ingrowth
22
23 523 of ^4He within the magma and assimilation of country rock rich in ^4He (Hilton et al., 1993; Hilton
24
25 524 et al., 2002; Tardani et al., 2016). The assimilation of radiogenic helium from country rocks,
26
27 525 representing the basement of the Quaternary volcanic edifices, has been previously identified in
28
29 526 Chilean Andes and exert a first order control on helium signatures in the magmatic sources and
30
31 527 fumaroles, which in turn is controlled by the structural contexts (Tardani et al., 2016; Veloso et al.,
32
33 528 2020; Rubidoux et al., 2020). Strontium isotopes, stable isotopes of water and $^4\text{He}/^{20}\text{Ne}$ ratio for
34
35 529 AF sample show that the water is largely dominated by a significant meteoric water contribution
36
37 530 in this area, which is consistent with the location, in the same area, of the groundwater recharge
38
39 531 zone. The COP-2 borehole intercepts the vapor-dominated geothermal reservoir at 1400 m depth,
40
41 532 and presents a helium ratio of 6.4Ra (Fig. 8). The $^{87}\text{Sr}/^{86}\text{Sr}$ ratio for COP-2 sample shows a
42
43 533 significant deviation from those of the Quaternary volcanic products of the CCVC, indicating the
44
45 534 presence of a radiogenic Sr source possibly from deeper-seated granitoids or from the Mesozoic
46
47 535 sedimentary basement, which is in agreement with the presence of radiogenic helium.
48
49
50
51
52
53
54
55
56
57
58
59

60 537 **6. CONCLUSIONS**

1
2
3
4
5
6
7
8
9
10
11
12
13
14
15
16
17
18
19
20
21
22
23
24
25
26
27
28
29
30
31
32
33
34
35
36
37
38
39
40
41
42
43
44
45
46
47
48
49
50
51
52
53
54
55
56
57
58
59
60
61
62
63
64
65

538 The proposed hydrological model of Copahue, including two sources of deep volatiles (Fig.
539 8), can explain the spatial distribution of helium isotopes in the CCVC, including the INSAR and
540 petrological data related to the magmatic sources in addition to the mapped and inferred structural
541 features in the area.

542 The main results of this study are the absence of young water, both in the reservoir (COP-
543 2 sample) and in the hydrological circuit feeding the shallow geothermal pools. The absence of
544 tritium and minimum ^{14}C age estimates of 13-14ka suggest that the hydrological circuit is more
545 complex than previously assumed (e.g., Agosto and Varekamp, 2016). This can have particular
546 consequences either for the exploitation of the shallow circuit for thermal balneation in the
547 Copahue Village and for the future exploitation of the field, for electricity production. The absence
548 of tritium in shallow hot springs indicate that the average residence time is higher than 70 years
549 and thus any future plan of balneotherapy expansion in the area need to take into account that
550 recharge can be slower than estimated, limiting the use - on the long term - for larger recreational
551 activities. The minimum ^{14}C residence time of 13-14ka suggest the presence of old waters together
552 with the meteoric recharge from the summit of the Copahue. The occurrence of old fluids is not
553 new in geothermal fields (e.g., Pinti et al., 2019) but need to be taken into account and
554 counterbalanced with a thoughtful plan of reinjection in case of future large-scale steam
555 exploitation for electricity production.

557 **Acknowledgements**

558 This study was funded by the ANID-FONDAP project 15090013 “Centro de Excelencia en
559 Geotermia de los Andes”, CEGA. Additional funding was provided by ANID-FONDECYT
560 Iniciación grant #11130351 and ANID-FONDECYT Regular grant #1201219. We wish to thank
561 the ANID-FONDEQUIP project EQM120098 for the trace element data obtained using the iCap

1
2
3
4
5
6
7
8
9
10
11
12
13
14
15
16
17
18
19
20
21
22
23
24
25
26
27
28
29
30
31
32
33
34
35
36
37
38
39
40
41
42
43
44
45
46
47
48
49
50
51
52
53
54
55
56
57
58
59
60
61
62
63
64
65

562 Q-ICP-MS equipment and Verónica Rodríguez and Erika Rojas at University of Chile for the fluid
563 chemical data acquisition. The authors thank A. Poirier, J.-F. Hélie, A. Valadez, and L. Richard at
564 GEOTOP for analyses of Sr, stable isotopes of water and CO₂, and noble gas isotopes, and for
565 handling of samples for ¹⁴C analysis. The authors also thank the “Ente Provincial Termas del
566 Neuquén” who granted permission to take samples for this study.

567

568

1
2
3
4
5
6
7
8
9
10
11
12
13
14
15
16
17
18
19
20
21
22
23
24
25
26
27
28
29
30
31
32
33
34
35
36
37
38
39
40
41
42
43
44
45
46
47
48
49
50
51
52
53
54
55
56
57
58
59
60
61
62
63
64
65

References

Aggarwal, P. K., Araguas-Araguas, L., Choudhry, M., van Duren, M., Froehlich, K., 2014. Lower groundwater ¹⁴C age by atmospheric CO₂ uptake during sampling and analysis. *Groundwater* 52, 20-24.

Agusto, M., Varekamp, J., 2016. The Copahue Volcanic-Hydrothermal System and Applications for Volcanic Surveillance, in: Tassi, F., Vaselli, O., Caselli, A.T. (Eds.), *Copahue Volcano*. Springer Berlin Heidelberg, Berlin, Heidelberg, pp. 199-238.

Agusto, M., Tassi, F., Caselli, A. T., Vaselli, O., Rouwet, D., Capaccioni, B., Caliro, S., Chiodini, G., Darrah, T., 2013. Gas geochemistry of the magmatic-hydrothermal fluid reservoir in the Copahue-Caviahue Volcanic Complex (Argentina). *J. Volcanol. Geotherm. Res.* 257, 44–56.

Allègre, C.J., Moreira, M., Staudacher, T., 1995. ⁴He/³He dispersion and mantle convection. *Geophys. Res. Lett.* 22, 2325-2328.

Barcelona, H., Yagupsky, D., Vigide, N., Senger, M., 2019. Structural model and slip-dilation tendency analysis at the Copahue geothermal system: Inferences on the reservoir geometry. *J. Volcanol. Geotherm. Res.* 375, 18-31.

Barcelona, H., Maffucci, R., Yagupsky, D., Senger, M., Bigi, S., 2020. Discrete fracture network model of the vapor zone leakages at the Copahue geothermal field. *J. Struct. Geol.* 140, 104155.

Benson, B.B., Krause Jr., D., 1980. Isotopic fractionation of helium during solution: a probe for the liquid state. *J. Solut. Chem.* 9, 895–909.

1
2
3
4
5
6
7
8
9
10
11
12
13
14
15
16
17
18
19
20
21
22
23
24
25
26
27
28
29
30
31
32
33
34
35
36
37
38
39
40
41
42
43
44
45
46
47
48
49
50
51
52
53
54
55
56
57
58
59
60
61
62
63
64
65

589

Birkle, P., Merkel, B., Portugal, E., Torres-Alvarado, I. S., 2001. The origin of reservoir fluids in the geothermal field of Los Azufres, Mexico: Isotopical and hydrological indications. Appl. Geochem. 16, 1595-1610.

593

Birkle, P., Portugal Marín, E., Pinti, D.L., Castro, M.C., 2016. Origin and evolution of geothermal fluids from Las Tres Vírgenes and Cerro Prieto fields, Mexico - Co-genetic volcanic activity and paleoclimatic constraints. Appl. Geochem. 65, 36-53.

596

Bonali F.L., Corazzato C., Bellotti F., Groppelli G., 2016. Active tectonics and its interactions with Copahue Volcano. In: Tassi F., Vaselli O., Caselli A. (eds) Copahue Volcano. Active Volcanoes of the World. Springer, Berlin, Heidelberg https://doi.org/10.1007/978-3-662-48005-2_2

600

Bowen, G.J., 2017. The online isotopes in precipitation calculator, v. 3.1, http://wateriso.utah.edu/waterisotopes/pages/data_access/oipc.html.

602

Cannatelli, C., Aracena, C., Leisen, M., Moncada, D., Roulleau, E., Vinet, N., Petrelli, M., Paolillo, A., Barra, F., Morata, D., 2016. Magma evolution at Copahue volcano (Chile/Argentina border): insights from melt inclusions. AGU Fall Meeting (Abstr.), 2016AGUFM.V31A3085C.

606

Chiodini, G., Allard, P., Caliro, S., Parello, F., 2000. ¹⁸O exchange between steam and carbon dioxide in volcanic and hydrothermal gases: implications for the source of water. Geochim. Cosmochim. Acta 64, 2479-2488.

1
2
3
4
5
6
7
8
9
10
11
12
13
14
15
16
17
18
19
20
21
22
23
24
25
26
27
28
29
30
31
32
33
34
35
36
37
38
39
40
41
42
43
44
45
46
47
48
49
50
51
52
53
54
55
56
57
58
59
60
61
62
63
64
65

609 Chiodini, G., Cardellini, C., Lamberti, M., Agosto, M., Caselli, A., Liccioli, C., Caliro, S., 2015.
610 Carbon dioxide diffuse emission and thermal energy release from hydrothermal systems at
611 Copahue–Caviahue Volcanic Complex (Argentina). *J. Volcanol. Geotherm. Res.* 304, 294-
612 303.

613 Craig, H., Lupton, J. E., Horibe, Y., 1978. A mantle helium component in Circum-Pacific volcanic
614 gases: Hakone, the Marianas, and Mt. Lassen. In: Alexander, Ozima, M. (Eds.), *Terrestrial*
615 *Rare Gases. Advances in Earth and Planetary Science.* Academic Publication, Japan, pp. 3–
616 16.

617 Crann, C.A., Murseli, S., St-Jean, G., Zhao, X., Clark, I.D., Kieser, W.E., 2017. First status report
618 on radiocarbon sample preparation at the A.E. Lalonde AMS Laboratory (Ottawa, Canada).
619 *Radiocarbon* 59, 695–704.

620 Fournier, R. O., Truesdell, A. H., 1970. Chemical indicators of subsurface temperature applied to
621 hot spring waters of Yellowstone National Park, Wyoming, USA. *Geothermics* 2, 529- 535.

622 Friedman, I., J.R. O'Neil 1977: Compilation of stable isotope fractionation factors of geochemical
623 interest. – In: *Data of Geochemistry 6th*, Geol. Surv. Prof. Paper 440–KK, p. 61.

624 Giggenbach, W.F., Stewart, M.K., 1982. Processes controlling the isotopic composition of steam
625 and water discharges from steam vents and steam-heated pools in geothermal areas.
626 *Geothermics* 11, 71–80.

627 Giggenbach, W. F., Goguel, R. L., 1989. Methods for the collection and analysis of geothermal and
628 volcanic water and gas samples. Department of Scientific and Industrial Research, Chemistry
629 Division. Petone, New Zealand.

1
2
3
4 630 Gizaw, B., 1996. The origin of high bicarbonate and fluoride concentrations in waters of the Main
5
6
7 631 Ethiopian Rift Valley, East African Rift system. *J. Afr. Earth Sci.* 22, 391-402.
8
9
10 632 Goff, F., Janik, C. J., 2000. Geothermal systems. *Encyclopedia of volcanoes*, John Wiley & Son,
11
12 633 817-834.
13
14
15
16 634 Goff, F., McMurtry, G.M., 2000. Tritium and stable isotopes of magmatic waters. *J. Volcanol.*
17
18
19 635 *Geotherm. Res.* 97, 347-396.
20
21
22 636 Heemskerk, A. R., Johnson, J., 1998. Tritium analysis: technical procedure 1.0. University of
23
24 637 Waterloo, Waterloo, ON.
25
26
27
28 638 Hilton D. R., Hammerschmidt K., Teufel S., Friedrichsen H., 1993. Helium isotope characteristics
29
30 639 of Andean geothermal fluids and lavas. *Earth Planet. Sci. Lett.* 120, 265–282.
31
32
33
34
35 640 Hilton D. R., Fischer T. P., Marty B., 2002. Noble gases and volatile recycling at subduction zones.
36
37 641 *Rev. Mineral. Geochem.* 47, 319–370.
38
39
40
41 642 Karolytè, R., Serno, S., Johnson, G., Gilfillan, S.M.V., 2017. The influence of oxygen isotope
42
43 643 exchange between CO₂ and H₂O in natural CO₂-rich spring waters: Implications for
44
45 644 geothermometry. *Appl. Geochem.* 84, 173-186.
46
47
48
49 645 Kitaoka, K., 1990. Water circulation rates in a geothermal field: a study of tritium in the Beppu
50
51 646 hydrothermal system, Japan. *Geothermics* 19, 515-539.
52
53
54
55 647 Javoy, M., Pineau, F., Delorme, H., 1986. Carbon and nitrogen isotopes in the mantle. *Chem. Geol.*
56
57 648 57, 41-62.
58
59
60
61
62
63
64
65

1
2
3
4 649 JICA, 1992. The feasibility study on the northern Neuquen geothermal development project. Japan
5
6
7 650 International Cooperation Agency, Neuquen, p. 444.
8
9
10 651 Lamberti, M. C., Vigide, N., Venturi, S., Agosto, M., Yagupsky, D., Winocur, D., Barcelona, H.,
11
12 652 Velez, M., Cardellini, Tassi, F., 2019. Structural architecture releasing deep-sourced carbon
13
14
15 653 dioxide diffuse degassing at the Caviahue–Copahue Volcanic Complex. *J. Volcanol.*
16
17 654 *Geotherm. Res.* 374, 131-141.
18
19
20
21 655 Linares, E., Oстера, H.A., Mas, L., 1999. Cronologia Potasio-Argon del complejo efusivo Copahue–
22
23 656 Caviahue, Provincia de Neuquen. *Rev. Asoc. Geol. Argent.* 54 (3), 240–247.
24
25
26
27 657 Lundgren, P., Nikkhoo, M. Samsonov, S.V., Milillo, P., Gil-Cruz, F., Lazo, J., 2017. Source model
28
29 658 for the Copahue volcano magma plumbing system constrained by InSAR surface
30
31 659 deformation observations, *J. Geophys. Res.: Solid Earth* 122, 5729–5747.
32
33
34
35
36 660 Mas, L.C., Mas, G.R., Bengochea, L., 2000. Heat flow of Copahue geothermal field; its relation
37
38 661 with tectonic scheme. *Proc. World Geother. Congr. Kyoto-Beppu, Japan*, pp. 1419-1424.
39
40
41
42 662 Mas, G., Mas, L., Bengochea, L., 1995. Zeolite zoning in drill holes of the Copahue geothermal
43
44 663 field, Neuquén, Argentina. *Proc. World Geother. Congr.*,1077-1081.
45
46
47
48 664 Mas, L.C., 2005. Present status of the Copahue geothermal project. *Proc. World Geother. Congr.*,
49
50 665 Antalya, Turkey, pp. 1–10.
51
52
53
54 666 Mason, E., Edmonds, M., Turchyn, A.V., 2017. Remobilization of crustal carbon may dominate
55
56 667 volcanic arc emissions. *Science* 357, 290-294
57
58
59
60 668 Maydagan, L., Franchini, M., Chiaradia, M., Bouhier, V., Di Giuseppe, N., Rey, R., Dimieri, L.,
61
62
63
64
65

1
2
3
4 669 2016. Petrogenesis of Quebrada de la Mina and Altar North porphyries (Cordillera of San
5
6 670 Juan, Argentina): Crustal assimilation and metallogenic implications. *Geosci. Frontiers* 8,
7
8
9 671 doi:10.1016/j.gsf.2016.11.011.
10
11
12 672 Melnick, D., Folguera, A., Ramos, V. A., 2006. Structural control on arc volcanism: the Copahue-
13
14
15 673 Agrio complex, South-Central Andes (37°50'S). *J. South Am. Earth Sci.* 22, 66–88.
16
17
18
19 674 Morata, D., Reich, M., Muñoz-Saez, C., Daniele, L., Rivera, G., Volpi, G., Ceccioni, M., Guidetti,
20
21 675 G., Cappetti, G., 2019. Origin and age of fluids at the Cerro Pabellón geothermal system,
22
23 676 Northern Chile. *Proceedings 41st New Zealand Geothermal Workshop, 25-27 November*
24
25
26 677 2019, Auckland, New Zealand.
27
28
29
30 678 Morrison P., Pine J., 1955. Radiogenic origin of the helium isotopes in rock. *Ann. N Y Acad. Sci.*
31
32 679 62, 71–92.
33
34
35
36 680 Nakanishi, S., Abe, M., Todaka, N., Yamada, M., Sierra, J., Gingsins, M., Pedro, G., 1995. Copahue
37
38 681 geothermal system, Argentina: study of a vapor-dominated reservoir. *Proc. World Geother.*
39
40
41 682 Congr., Florence, Italy, pp. 18-31.
42
43
44 683 Notsu, K., Wakita, H., Nakamura, Y., 1991. Strontium isotopic composition of hot spring and
45
46
47 684 mineral spring waters, Japan. *Appl. Geochem.* 6, 543-551.
48
49
50
51 685 Panarello, H.O., 2002. Características isotópicas y termodinámicas de reservorio del campo
52
53 686 geotérmico Copahue-Caviahue, provincia del Neuquén. *Rev. Asoc. Geol. Argentina* 57, 182-
54
55 687 194.
56
57
58
59 688 Panichi, C., Ferrara, G., Gonfiantini, R., 1977. Isotope geothermometry in the Larderello
60
61
62
63
64
65

1
2
3
4 689 geothermal field. *Geothermics* 5, 81–88.
5
6
7
8 690 Pinti, D.L., Castro, M.C., López-Hernández, A., Hernández Hernández, M.A., Richard, L., Hall,
9
10 691 C.M., Shouakar-Stash, O., Flores-Armenta, M., Rodríguez-Rodríguez, M.H., 2019. Cerro
11
12 692 Prieto Geothermal Field (Baja California, Mexico) – A fossil system? Insights from a noble
13
14
15 693 gas study. *J. Volcanol. Geotherm. Res.* 371, 32-45.
16
17
18
19 694 Reimer, P. J., Brown, T. A., Reimer, R. W., 2004. Discussion: reporting and calibration of post-
20
21 695 bomb ¹⁴C data. *Radiocarbon* 46, 1299-1304.
22
23
24
25 696 Richard, L., Pinti, D.L., Hélie, J.-F., Hernández, A.L., Shibata, T., Castro, M.C., Sano, Y.,
26
27 697 Shouakar-Stash, O., Sandoval-Medina, F., 2019. Variability of deep carbon sources in
28
29
30 698 Mexican geothermal fluids. *J. Volcanol. Geother. Res.* 370, 1-12.
31
32
33
34 699 Richet, P., Bottinga, Y., Javoy, M., 1977. A Review of Hydrogen, Carbon, Nitrogen, Oxygen,
35
36 700 Sulphur, and Chlorine Stable Isotope Fractionation Among Gaseous Molecules. *Annu. Rev.*
37
38 701 *Earth Planet. Sci.* 5, 65–110.
39
40
41
42 702 Robidoux, P., Rizzo, A.L., Aguilera, F., Aiuppa, A., Artale, M., Liuzzo, M., Nazzari, M., Zummo,
43
44 703 F., 2020. Petrological and noble gas features of Lascar and Lastarria volcanoes (Chile):
45
46
47 704 Inferences on plumbing systems and mantle characteristics. *Lithos* 370-371.
48
49
50
51 705 Roulleau, E., Tardani, D., Sano, Y., Takahata, N., Vinet, N., Bravo, F., Muñoz, C., Sanchez, J.,
52
53 706 2016. New insight from noble gas and stable isotopes of geothermal/hydrothermal fluids at
54
55 707 Cavihue-Copahue Volcanic Complex: Boiling steam separation and water-rock interaction
56
57
58 708 at shallow depth. *J. Volcanol. Geotherm. Res.* 328, 70-83.
59
60
61
62
63
64
65

1
2
3
4
5
6
7
8
9
10
11
12
13
14
15
16
17
18
19
20
21
22
23
24
25
26
27
28
29
30
31
32
33
34
35
36
37
38
39
40
41
42
43
44
45
46
47
48
49
50
51
52
53
54
55
56
57
58
59
60
61
62
63
64
65

709 Roulleau, E., Bravo, F., Pinti, D.L., Barde-Cabusson, S., Pizarro, M., Tardani, D., de la Cal, F.,
710 2017. Structural controls on fluid circulation at the Caviahue-Copahue Volcanic Complex
711 (CCVC) geothermal area (Chile-Argentina), revealed by soil CO₂ and temperature, self-
712 potential, and helium isotopes. *J. Volcanol. Geotherm. Res.* 341, 104-118.

713 Roulleau, E., Tardani, D., Vlastelic, I., Vinet, N., Sanchez, J., Sano, Y., Takahata, N., 2018. Multi-
714 element isotopic evolution of magmatic rocks from Caviahue-Copahue Volcanic Complex
715 (Chile-Argentina): Involvement of mature slab recycled materials. *Chem. Geol.* 476, 370-
716 388.

717 Rowe Jr., G.L., Brantley, S.L., Fernandez, J.F., Borgia, A., 1995. The chemical and hydrologic
718 structure of Poás Volcano, Costa Rica. *J. Volcanol. Geotherm. Res.* 64, 233-267.

719 Sielfeld, G., Cembrano, J., Lara, L., 2017. Transtension driving volcano-edifice anatomy: Insights
720 from Andean transverse-to-the-orogen tectonic domains. *Quatern. Int.* 438, 33-49.

721 Sierra, J.L., Pedro, G., D'Amore, F., Panarello, H., 1992. Reservoir characteristics of the vapor
722 dominated geothermal field of Copahue, Neuquen, Argentina, as established by isotopic and
723 geochemical techniques, International Atomic Energy Agency (IAEA), pp. 13-30.

724 Smith, S.P., Kennedy, B.M., 1983. The solubility of noble gases in water and NaCl brine. *Geochim.*
725 *Cosmochim. Acta* 47, 503-515.

726 Stefánsson, A., Arnórsson, S., 2005. The geochemistry of As, Mo, Sb and W in natural geothermal
727 waters, Iceland. *Proc. World Geother. Congr., Antalaya, Turkey*, pp. 1-7.

728 Stuiver, M., Polach, H.A., 1977. Discussion: reporting of ¹⁴C data. *Radiocarbon* 19, 355–63.

1
2
3
4 729 Taran, Y., Zelenski, M., 2015. Systematics of water isotopic composition and chlorine content in
5
6 730 arc-volcanic gases. *Geol. Soc. London Spec. Publ.* 410, 237-262.
7
8
9
10 731 Tassi, F., Agosto, M., Lamberti, C., Caselli, A., Pecoraino, G., Caponi, C., Vaselli, O., 2017. The
11
12 732 2012–2016 eruptive cycle at Copahue volcano (Argentina) versus the peripheral gas
13
14 733 manifestations: hints from the chemical and isotopic features of fumarolic fluids. *Bull.*
15
16 734 *Volcanol.* 79, 69.
17
18
19
20
21 735 Thorpe, R.S., Francis, P.W., Harmon, R.S., Moorbath, S.E., Windley, B.F., 1981. Andean andesites
22
23 736 and crustal growth. *Phil. Trans. Royal Soc. London Series A* 301, 305-320.
24
25
26
27 737 Varekamp, J. C., DeMoor, J. M., Merrill, M. D., Colvin, A. S., Goss, A. R., 2006. Geochemistry
28
29 738 and isotopic characteristics of the Cavihue–Copahue volcanic complex, Province of
30
31 739 Neuquén, Argentina. *Geol. Soc. America Spec. Paper* 407, 317–342.
32
33
34
35
36 740 Veloso E., Tardani D., Elizalde D., Godoy B., Sánchez-Alfaro P., Aron F., Reich M., Morata D.A.,
37
38 741 2020. Review of the geodynamic constraints on the development and evolution of geothermal
39
40 742 systems in the Central Andean Volcanic Zone (18–28°Lat.S). *Intern. Geol. Rev.* 62, 1294-
41
42 743 1318
43
44
45
46
47 744
48
49
50
51 745
52
53
54 746
55
56
57
58 747
59
60
61
62
63
64
65

1
2
3
4
5
6
7
8
9
10
11
12
13
14
15
16
17
18
19
20
21
22
23
24
25
26
27
28
29
30
31
32
33
34
35
36
37
38
39
40
41
42
43
44
45
46
47
48
49
50
51
52
53
54
55
56
57
58
59
60
61
62
63
64
65

748 **FIGURE CAPTIONS**

749 **Figure 1.** Structural map of the CCVC. Solid and dashed lines represent main faults from Melnick
et al. (2006), Rojas Vera et al. (2009), Barcelona et al. (2019), and Lamberti et al. (2019). White
circles and squares represent the locations of sampled hot springs and wells respectively. Gray
circles represent the thermal springs located in the area, but not sampled as part of this study. AF:
Anfiteatro; CB: Cabañita; CC: Chanco-có; LM: Las Máquinas; LMM: Las Maquinitas; PM:
Pucón-Mahuida; TC: Termas de Copahue.

755 **Figure 2.** Sulfate contents versus trace element concentrations of Al (a), Fe (b), Mn (c), Rb (d), As
(e) and Cs (f) for the well COP-2 condensate (blue square) and hot spring waters (blue circles).

757 **Figure 3.** Relationship between the $1000 \ln \alpha$ (CO₂-H₂O) in volcanic and hydrothermal fluids
from the CCVC and their emission temperatures. The theoretical curves for equilibrium
fractionation between CO₂ and H₂O in the gas phase from Friedman and O'Neil, (1977) and Richet
et al. (1977), and the polynomial best fit representing the volcanic and hydrothermal fluids
(Chiodini et al., 2000) are reported for comparison.

762 **Figure 4.** $\delta^2\text{H}$ versus (CO₂-corrected-) $\delta^{18}\text{O}$ of the CCVC sampled hot spring waters and COP-2
well condensate. The stable isotopic composition of geothermal pools (gray circles), local
meteoric water line (LMWL) and evaporation line (EVAP) are from Augusto and Varekamp
(2016). The andesitic water and magmatic water fields, as defined by Taran and Zelenski (2015),
are also indicated, together with meteoric water endmember (green star; Panarello, 2002) and
those calculated using OIPC at Copahue summit (light blue star) and at 1600m elevation (dark
blue) (Augusto and Varekamp, 2016).

769 **Figure 5.** Strontium isotope ratios ($^{87}\text{Sr}/^{86}\text{Sr}$) versus the temperature of the sampled fluids (in °C)
(a), SiO₂ contents (b) and the $\delta^{13}\text{C}$ -CO₂ (c). The orange area (labelled “local volcanics”)

1
2
3
4
5
6
7
8
9
10
11
12
13
14
15
16
17
18
19
20
21
22
23
24
25
26
27
28
29
30
31
32
33
34
35
36
37
38
39
40
41
42
43
44
45
46
47
48
49
50
51
52
53
54
55
56
57
58
59
60
61
62
63
64
65

771 represents the range of measured $^{87}\text{Sr}/^{86}\text{Sr}$ values in local Copahue volcanic rocks (data from
772 Varekamp et al., 2006 and Roulleau et al., 2018).

773 **Figure 6.** R/Ra versus $^4\text{He}/^{20}\text{Ne}$ of CCVC samples from this study and fumarole samples from
774 Roulleau et al. (2016). The MORB, crust, Air and Air-Saturated Water (ASW) endmembers are
775 reported. Dashed lines represent only mixing curves between mantle, crust, and ASW endmembers.

776 **Figure 7.** $^4\text{He}/^{20}\text{Ne}$ ratio versus $\delta^2\text{H}$ (a) and DOC/DIC ratio (b). The water ages measured using
777 ^{14}C are reported for LM, COP-2, and TC samples.

778 **Figure 8.** Block model showing the structurally-controlled fluid circulation proposed for the
779 CCVC. Black lines represent the main and secondary faults and fractures from Melnick et al.
780 (2006), Rojas Vera et al. (2009), Barcelona et al. (2019), and Lamberti et al. (2019). The geometry
781 and orientation of deep and shallow magmatic reservoirs are reported as proposed by Lundgren et
782 al. (2017). The geothermal reservoir is reported as described by Barcelona et al. (2019). Blue,
783 orange, and red arrows represent the ascent pathways of hydrothermal fluids with low (4.5 to 5.5
784 Ra), intermediate (5.6 to 6.9 Ra), and high helium (7.0 to 9.0 Ra) ratios respectively.

1
2
3
4 790
5
6
7
8
9
10
11
12
13
14
15
16
17
18
19
20
21
22
23
24
25
26
27
28
29
30
31
32
33
34
35
36
37 791
38
39 792
40
41 793
42
43
44 794
45
46 795
47
48
49 796
50
51 797
52
53 798
54
55
56 799
57
58
59
60
61
62
63
64
65

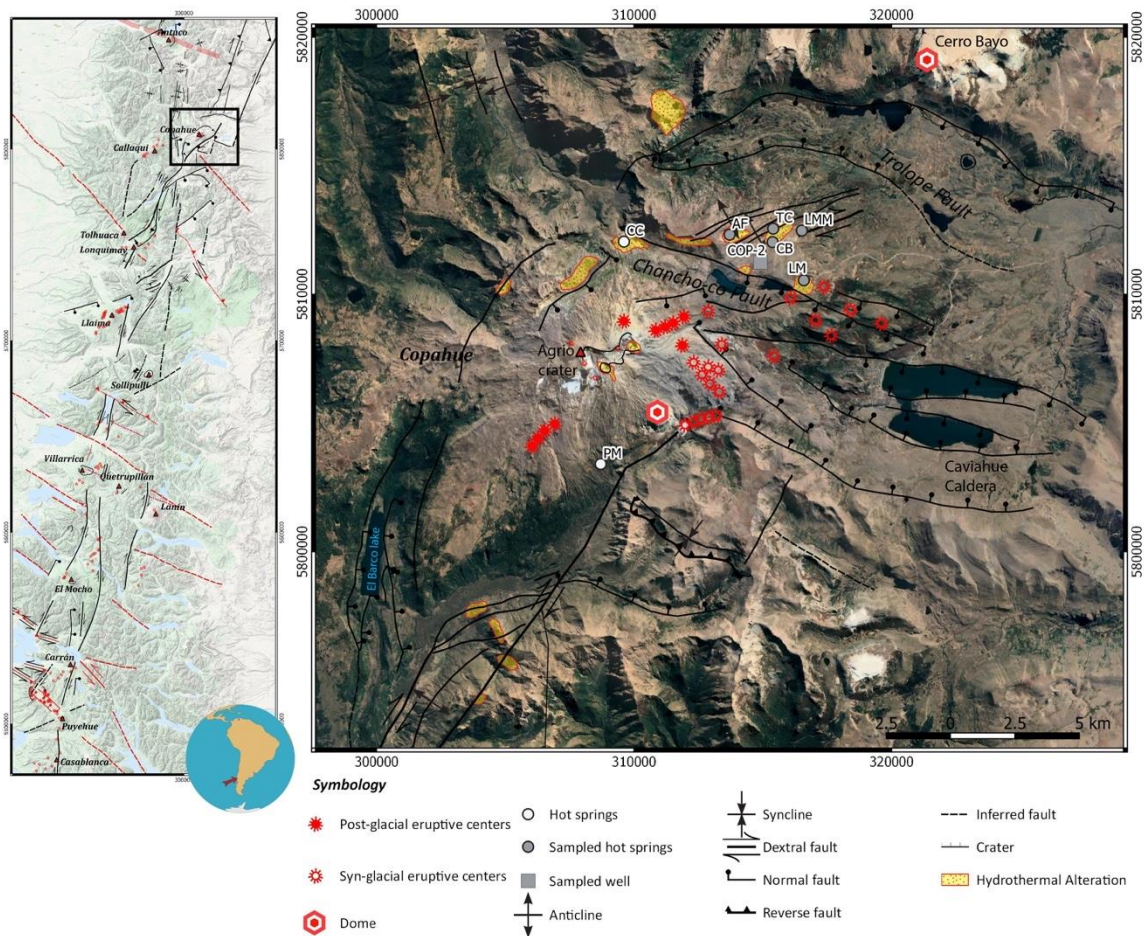
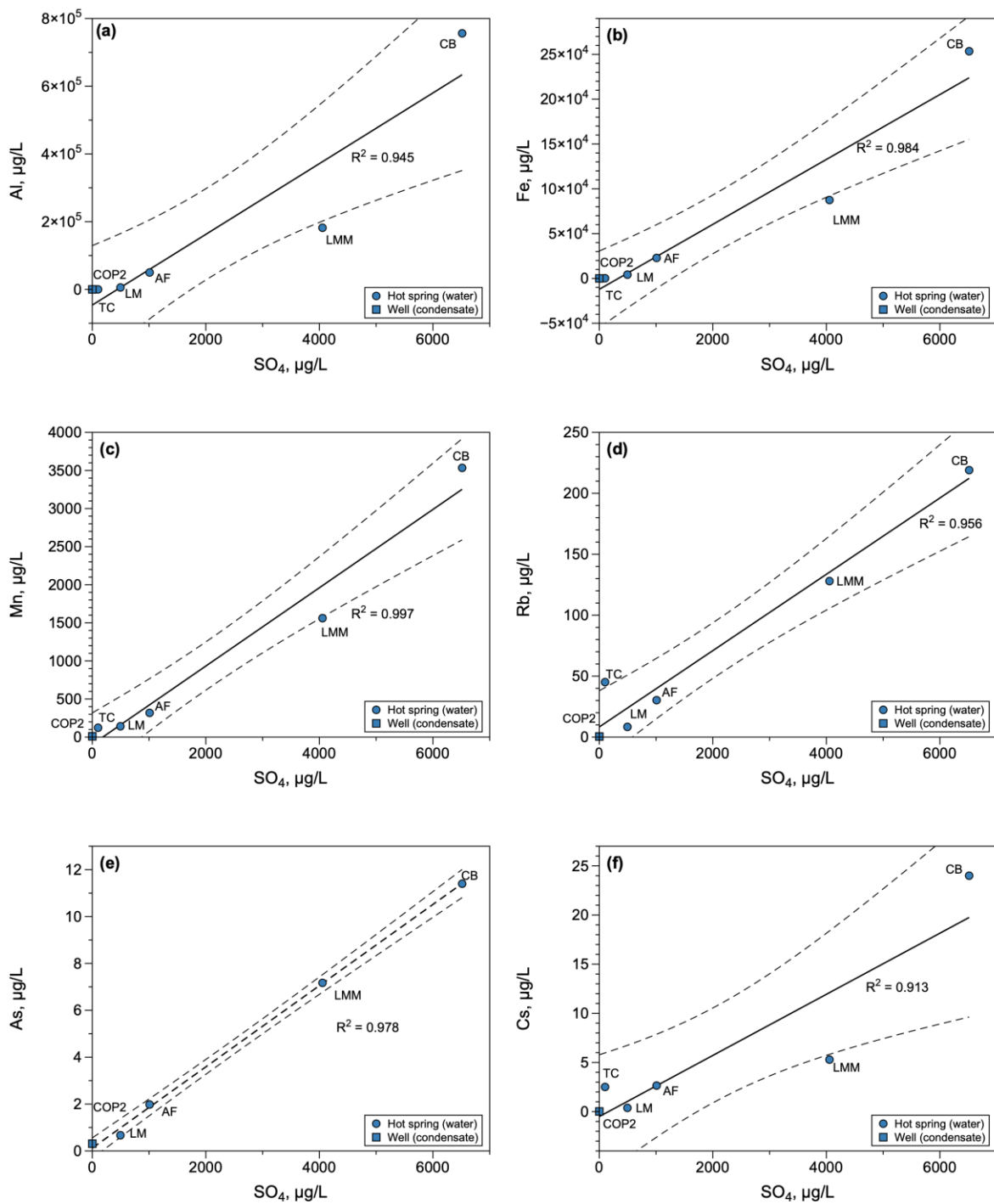


Figure 1

1
2
3
4
5
6
7
8
9
10
11
12
13
14
15
16
17
18
19
20
21
22
23
24
25
26
27
28
29
30
31
32
33
34
35
36
37
38
39
40
41
42
43
44
45
46
47
48
49
50
51
52
53
54
55
56
57
58
59
60
61
62
63
64
65



800
801
802

Figure 2

1
2
3
4 803
5
6
7
8
9
10
11
12
13
14
15
16
17
18
19
20
21
22
23
24
25
26
27
28
29
30
31
32
33
34
35
36 804
37
38 805
39
40
41 806
42
43 807
44
45
46
47
48
49
50
51
52
53
54
55
56
57
58
59
60
61
62
63
64
65

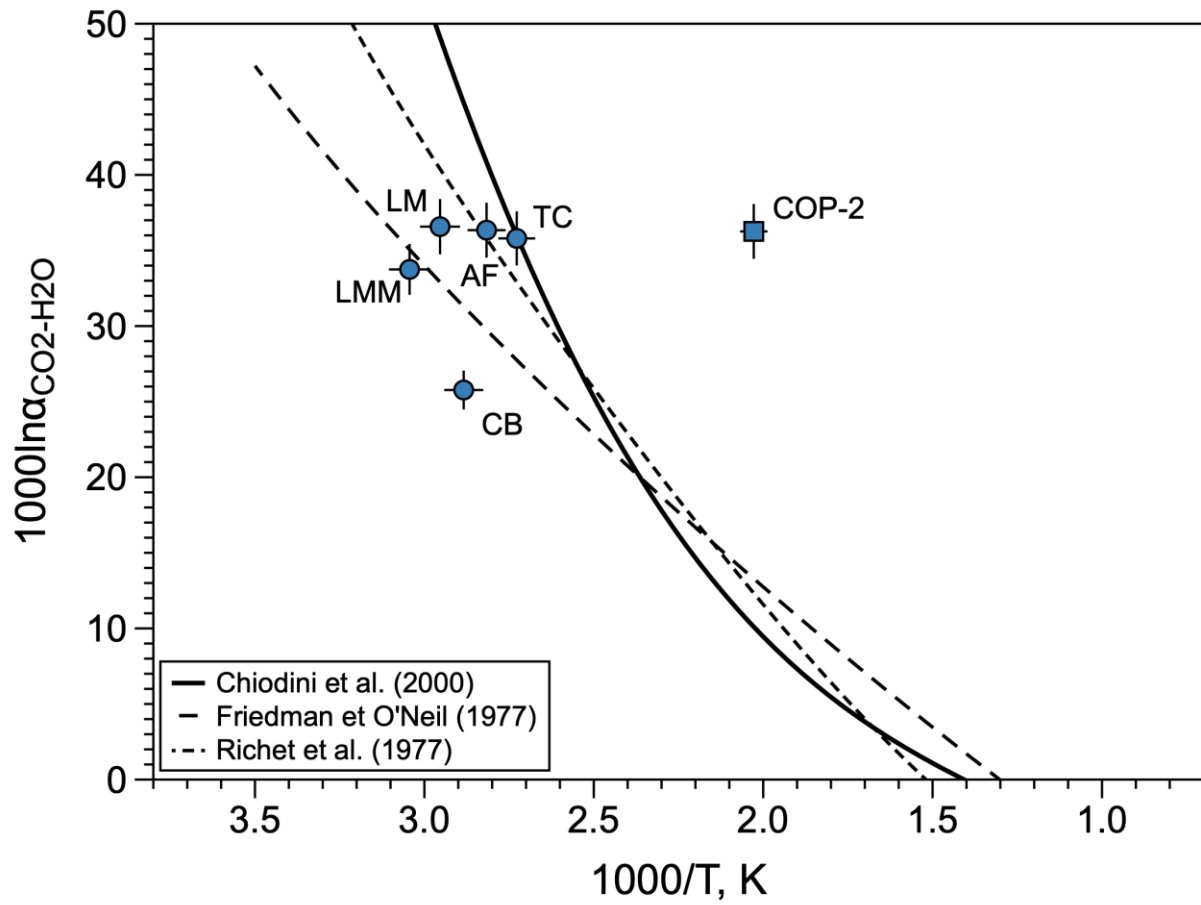


Figure 3

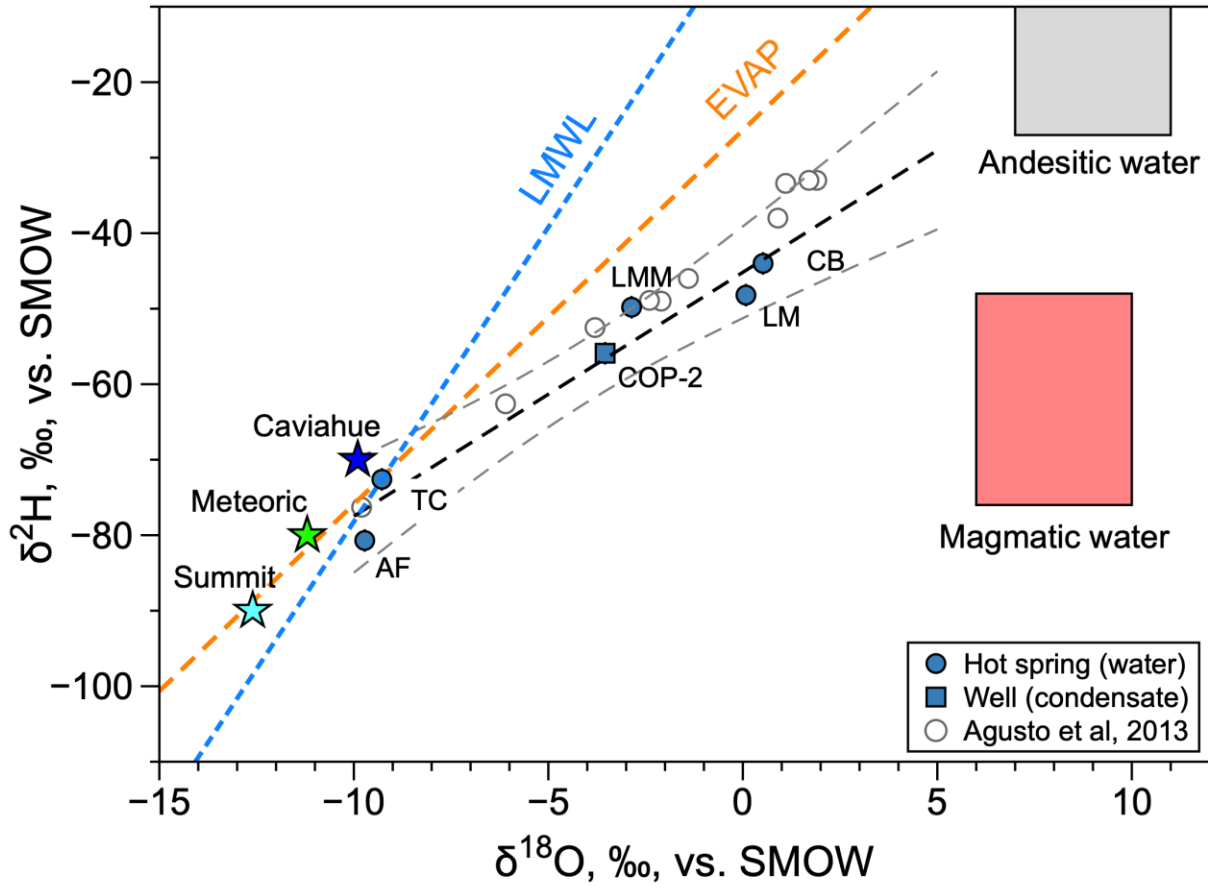
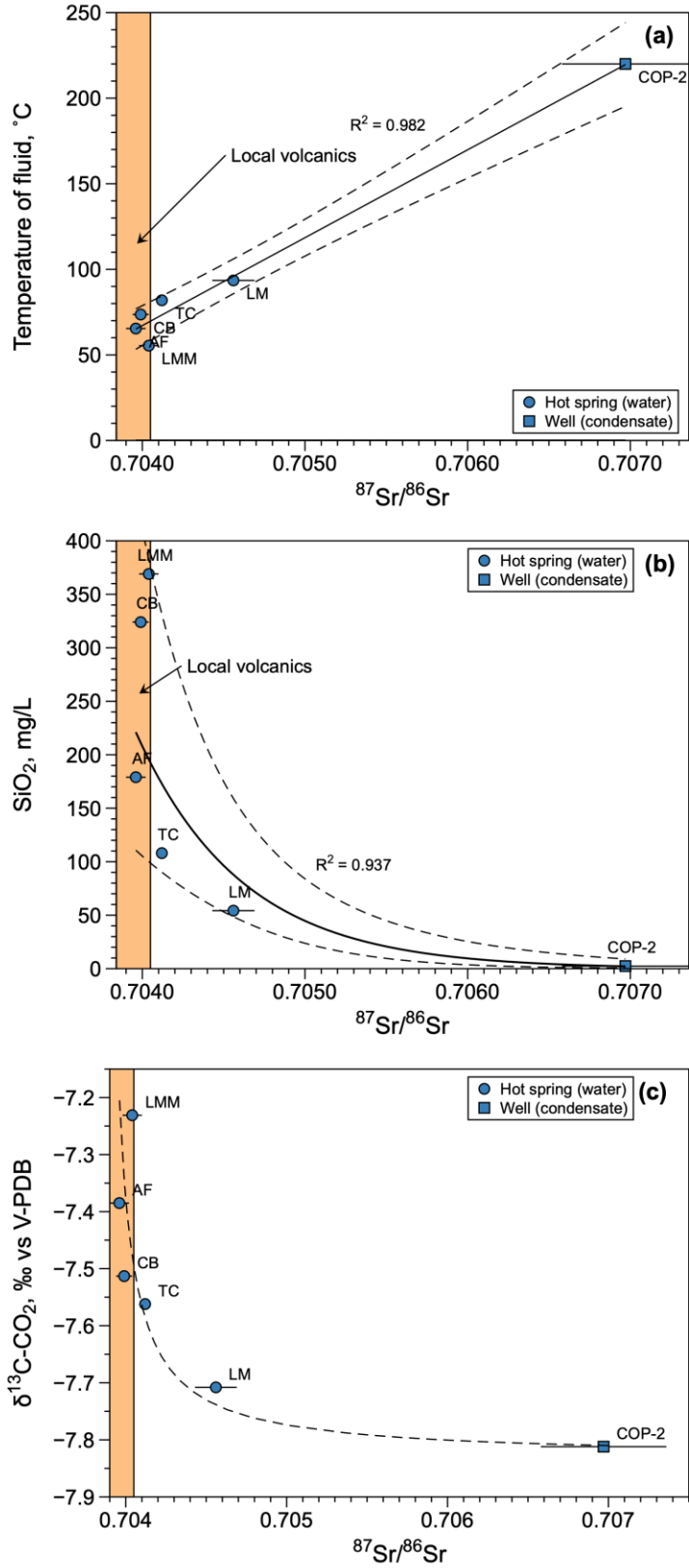


Figure 4



812

813 Figure 5

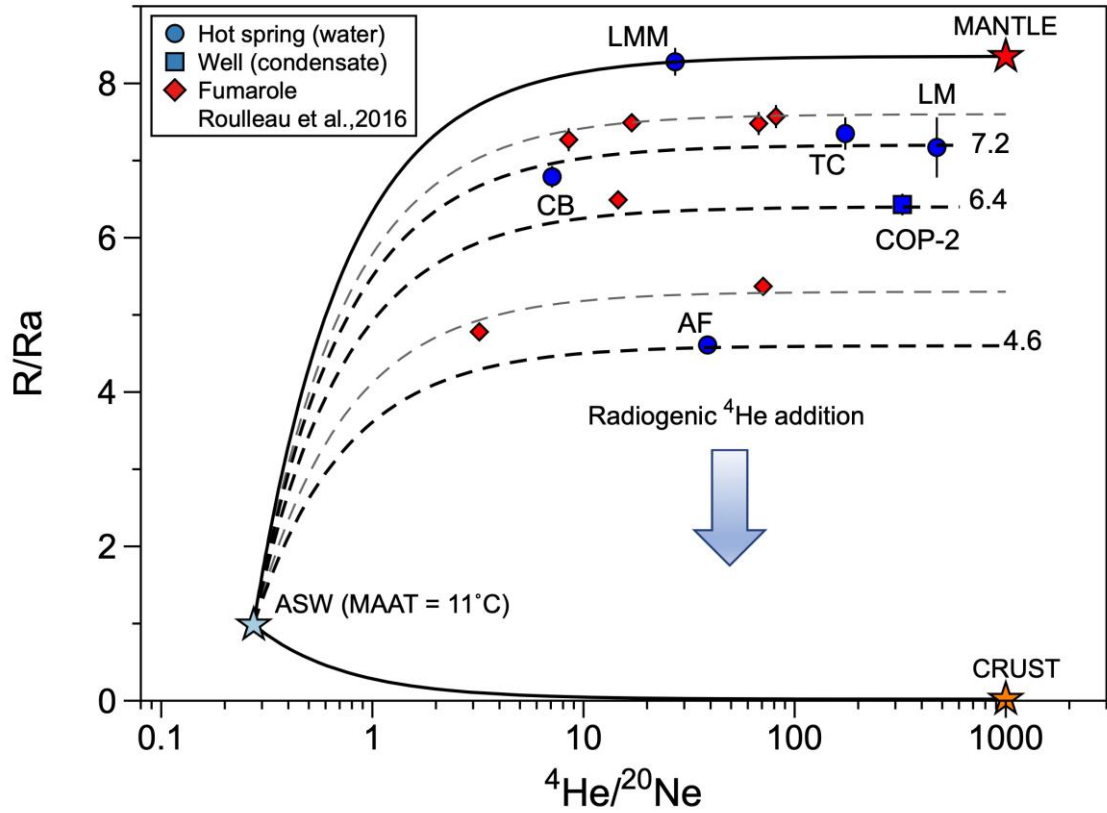
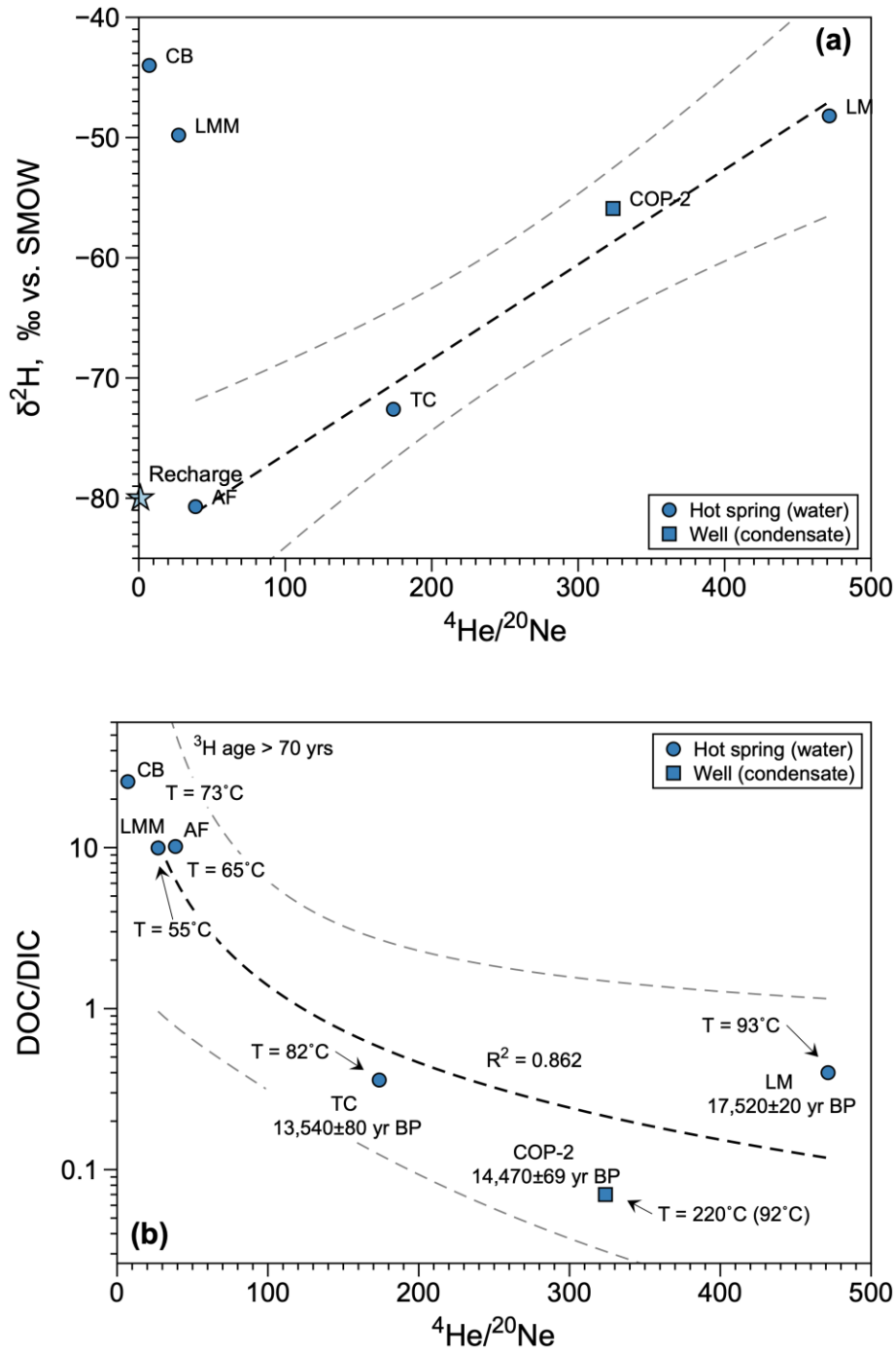


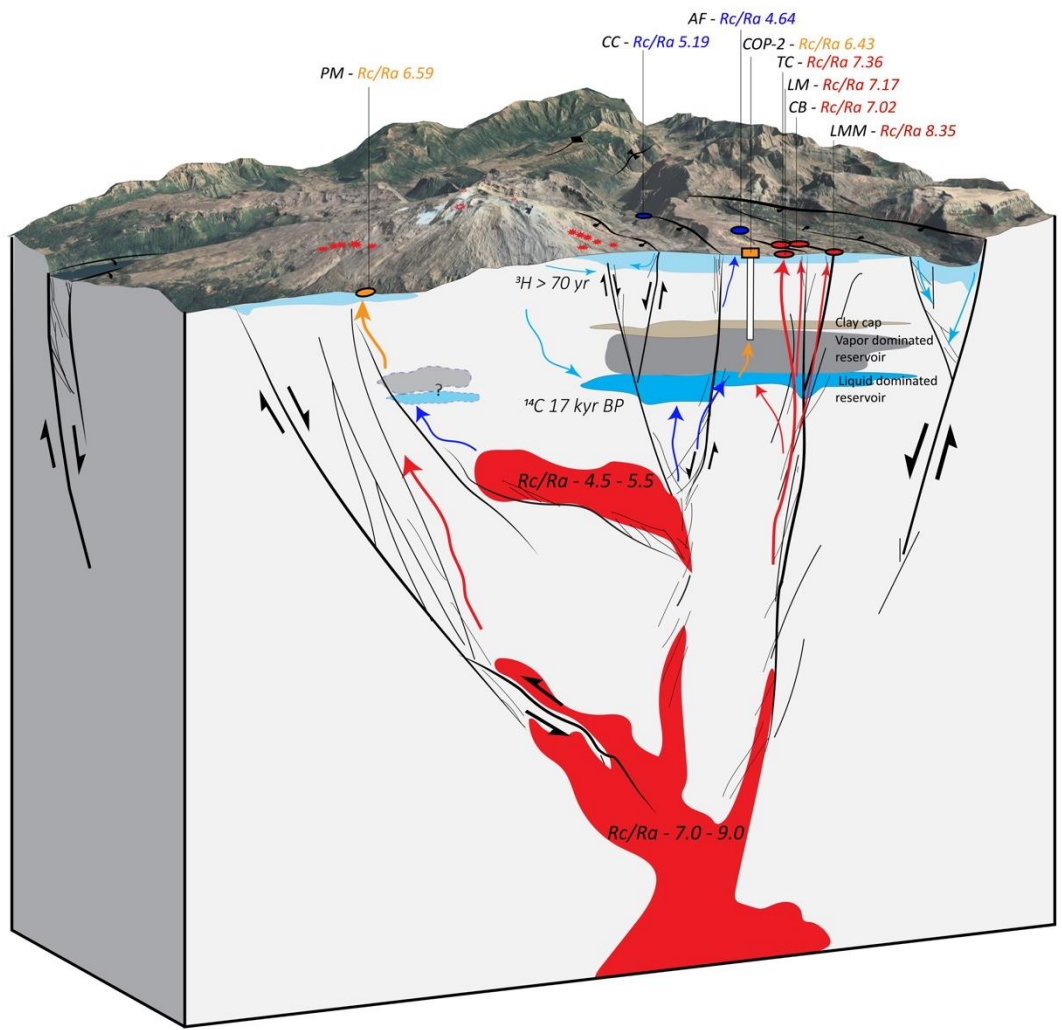
Figure 6

1
2
3
4
5
6
7
8
9
10
11
12
13
14
15
16
17
18
19
20
21
22
23
24
25
26
27
28
29
30
31
32
33
34
35
36
37
38
39
40
41
42
43
44
45
46
47
48
49
50
51
52
53
54
55
56
57
58
59
60
61
62
63
64
65



817
818 Figure 7

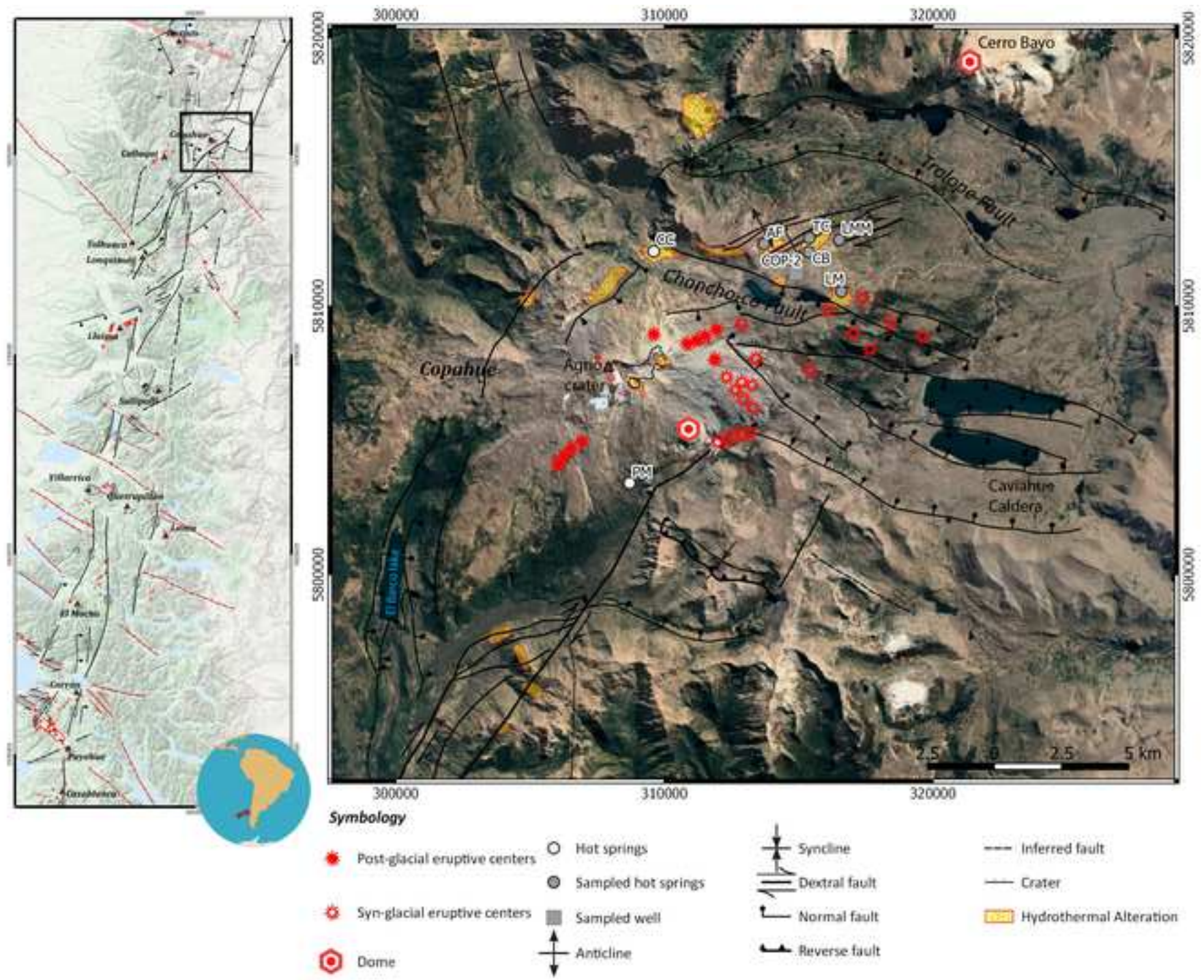
1
2
3
4 819
5
6
7
8
9
10
11
12
13
14
15
16
17
18
19
20
21
22
23
24
25
26
27
28
29
30
31
32
33
34
35
36
37
38
39
40

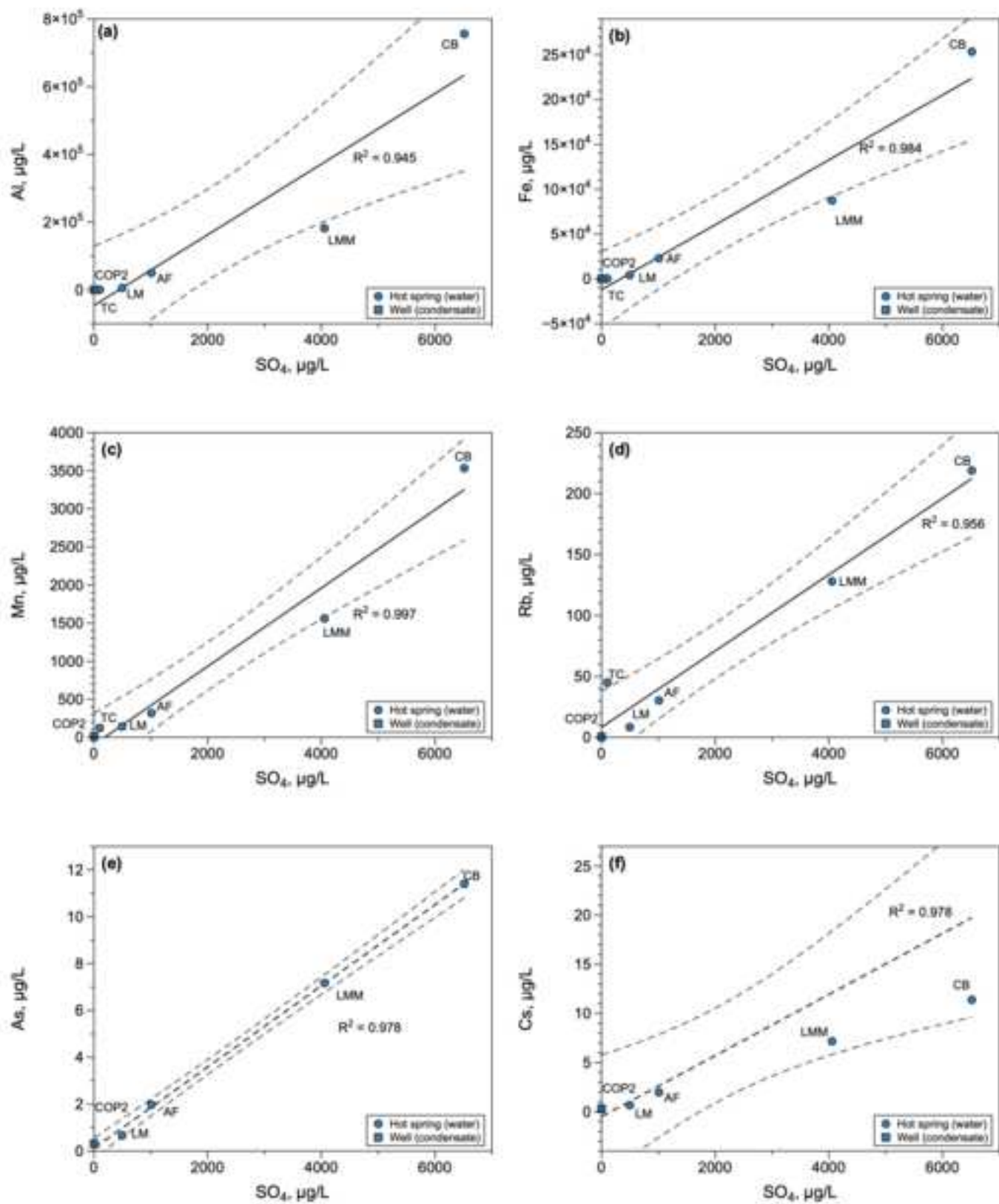


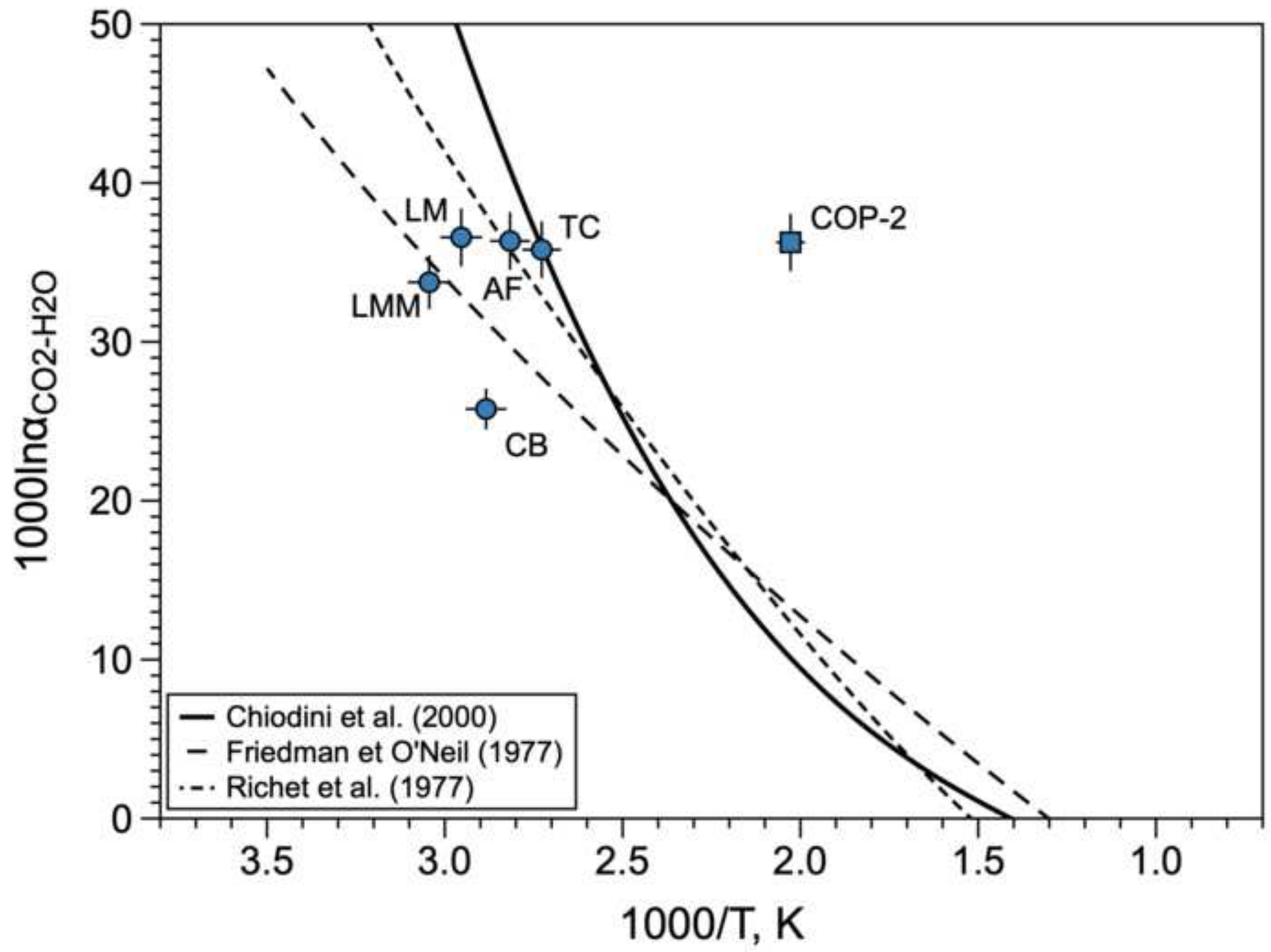
41 820

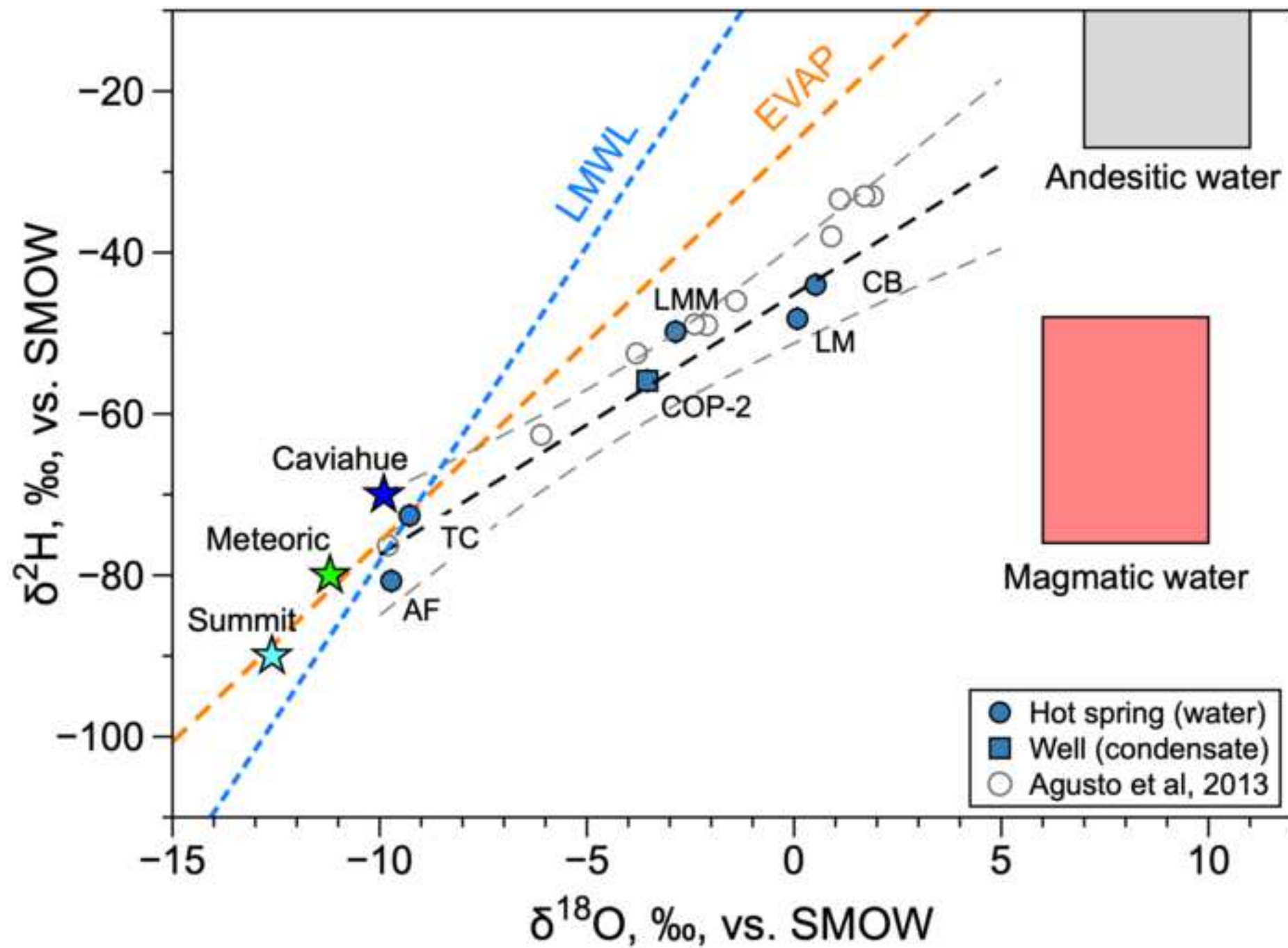
42
43
44 821 Figure 8

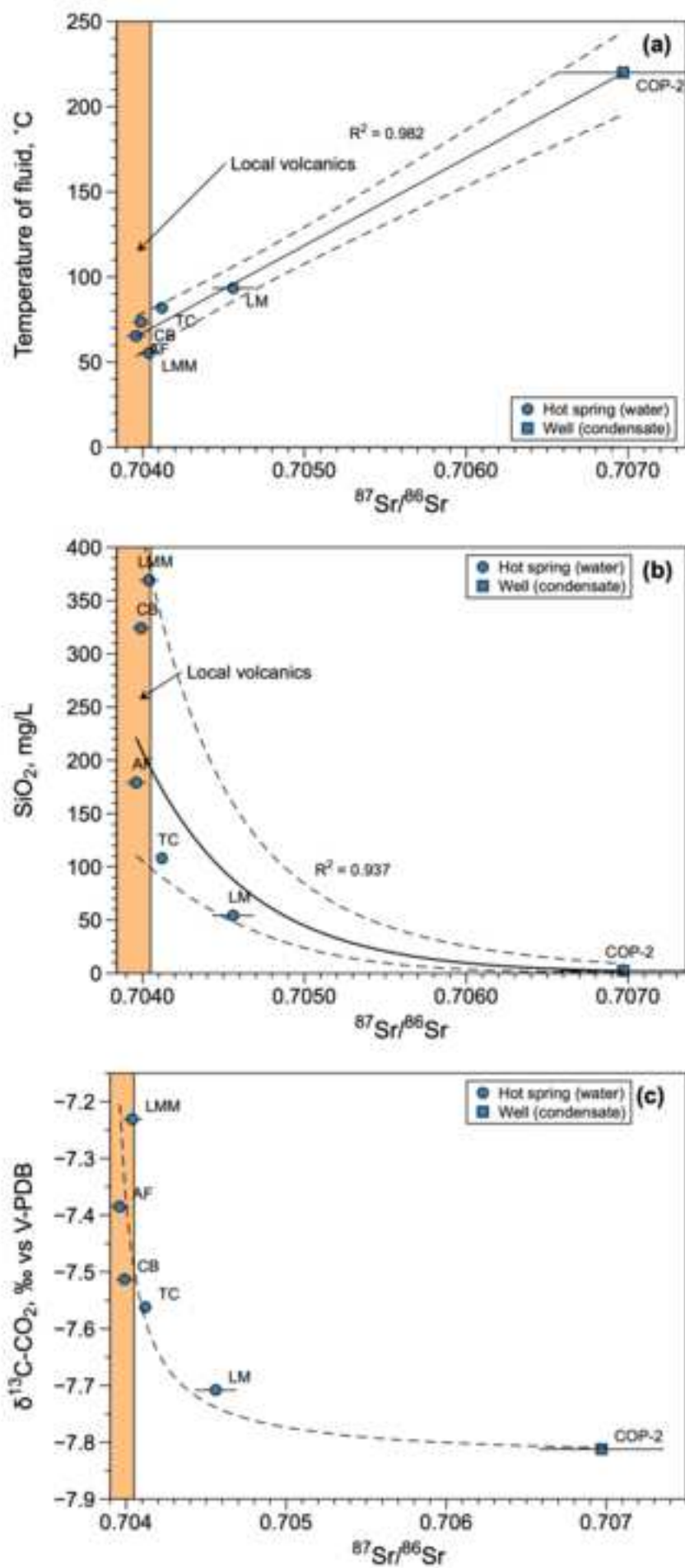
45
46
47
48
49
50
51
52
53
54
55
56
57
58
59
60
61
62
63
64
65

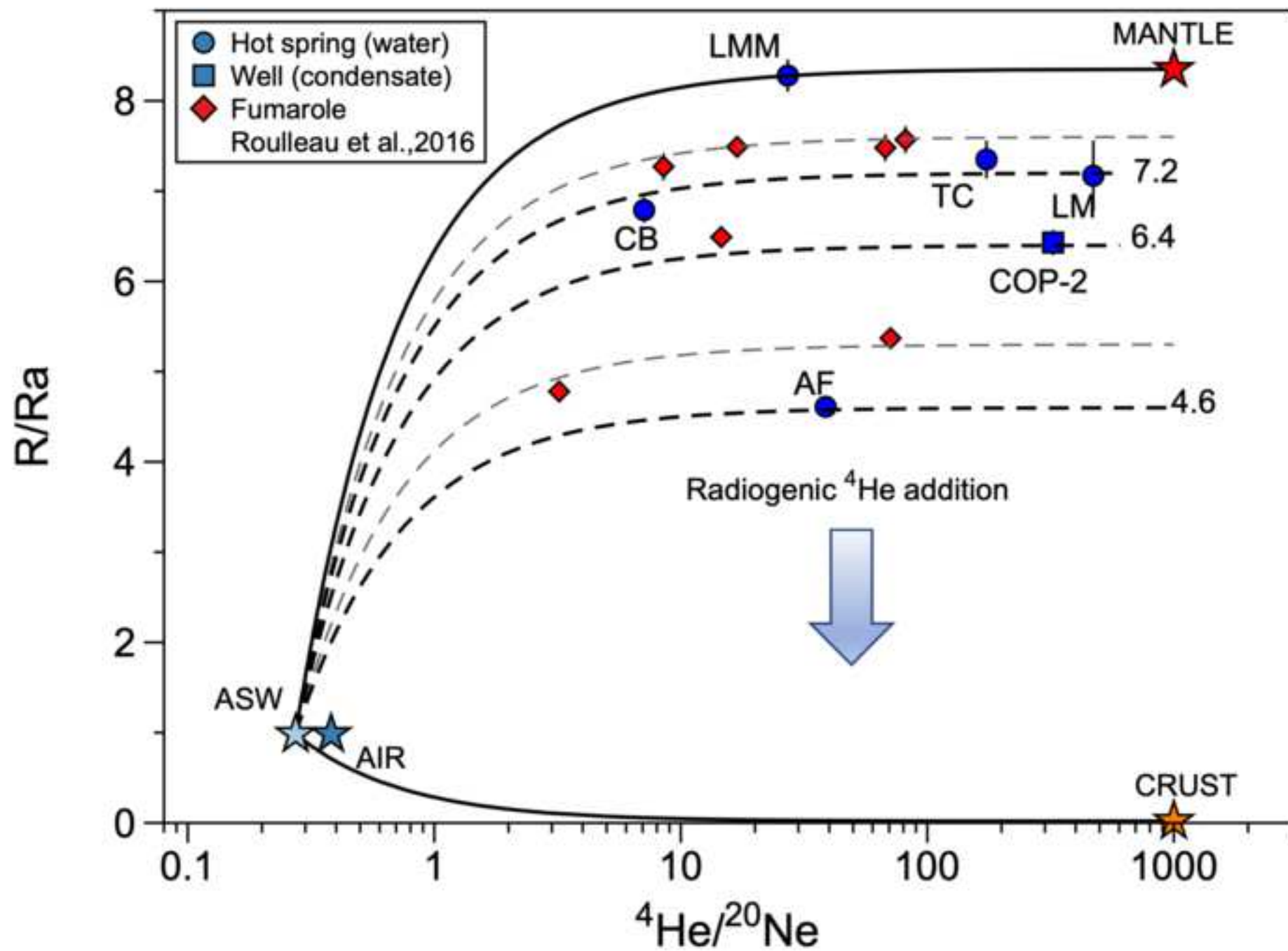


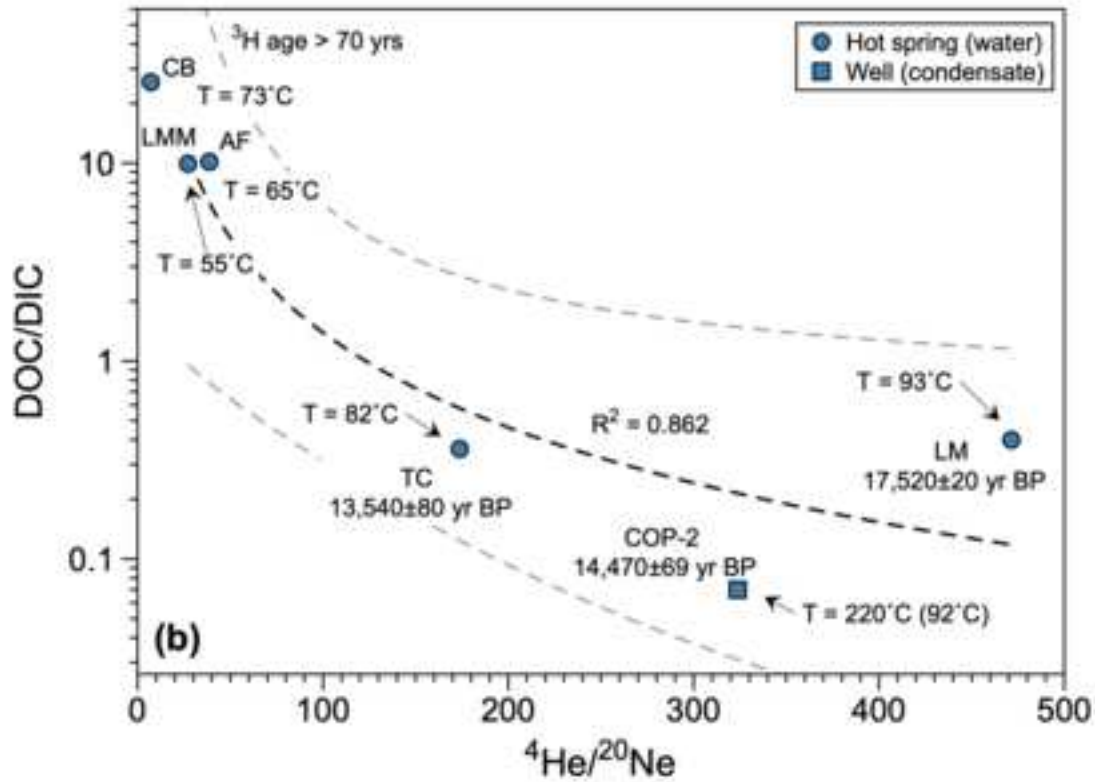
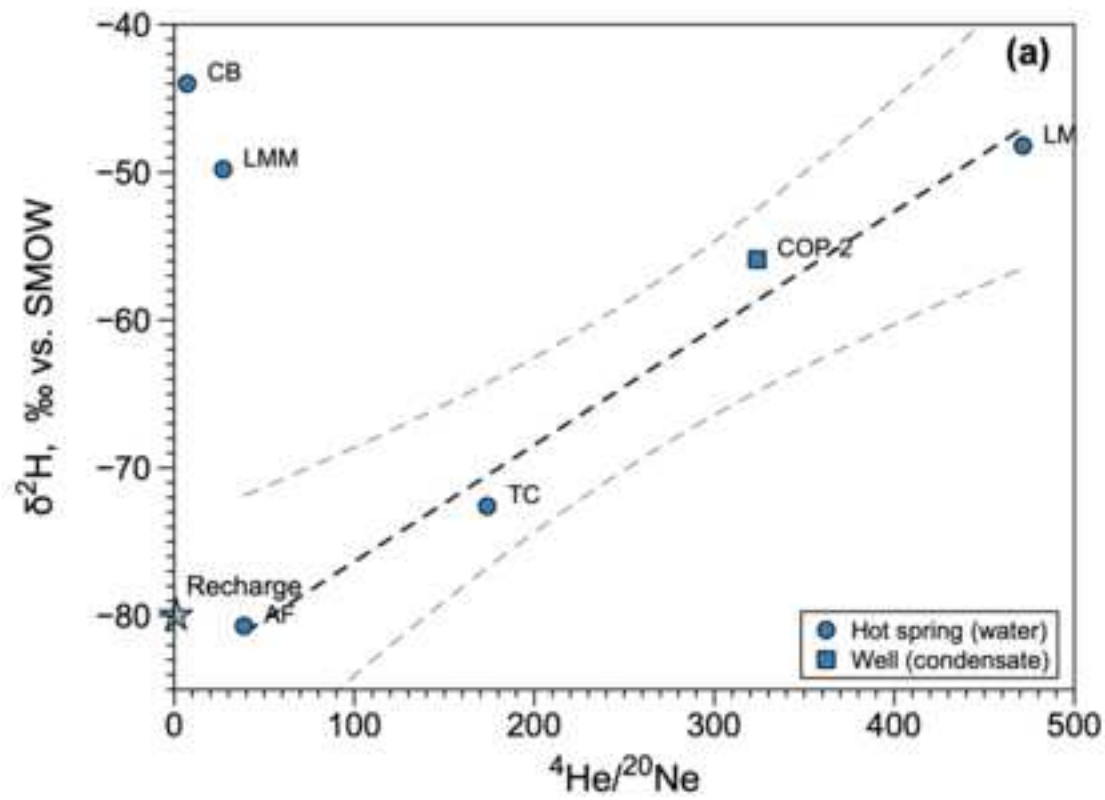












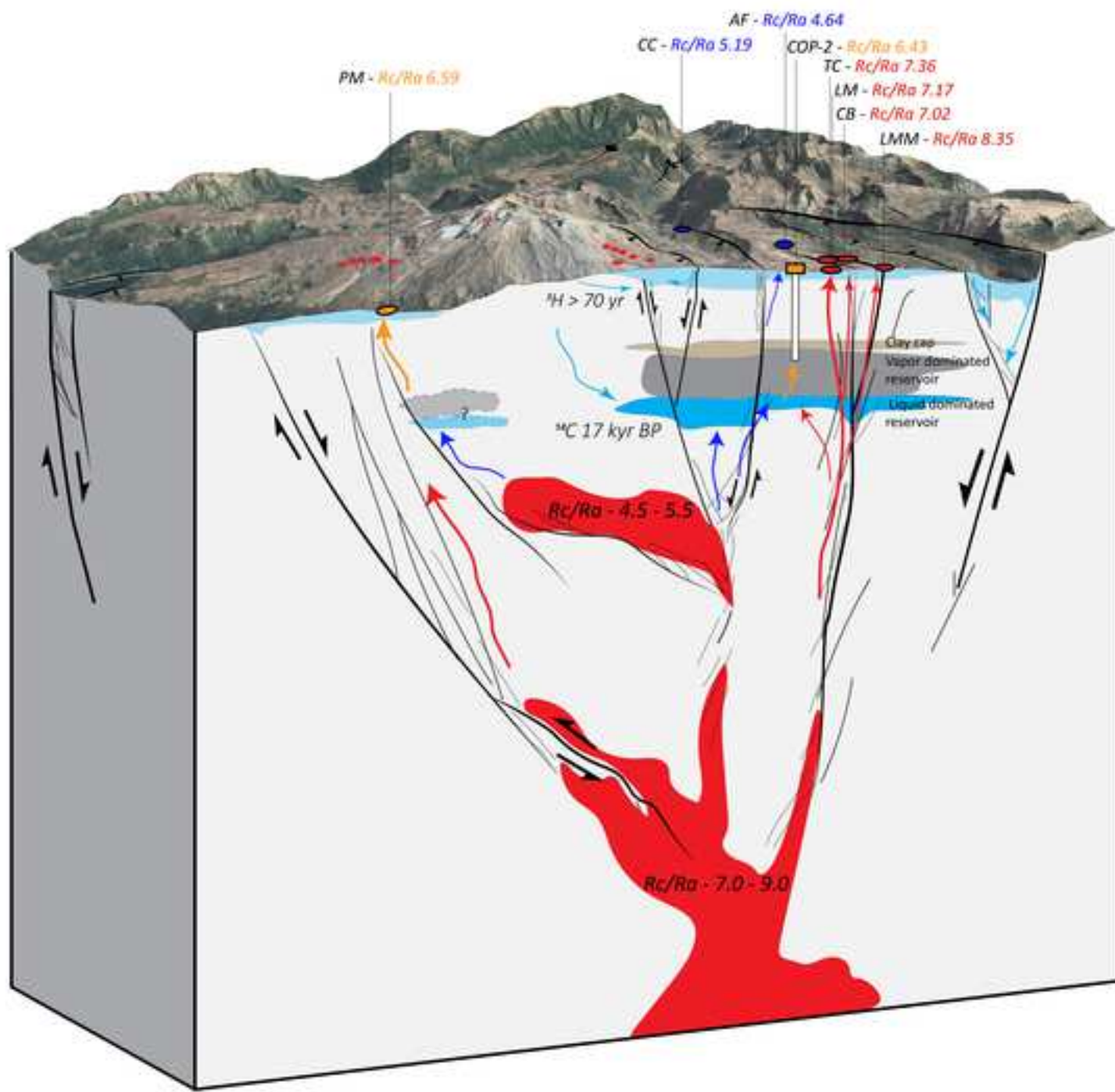


Table 1. Ionic concentrations in water and condensate samples from Copahue thermal area.

Sample	Location name	Type	Longitude E WG84, m	Latitude S WG84, m	Altitude m.s.l.	T °C	pH -
LM	Las Máquinas	Hot spring	316599	5810539	1979	93.5	2.26
TC	Termas Copahue	Hot spring	315412	5812554	2013	81.9	6.8
LMM	Las Maquinitas	Hot spring	316522	5812479	2021	55.4	1.9
AF	Anfiteatro	Hot spring	313708	5812321	2152	65.4	2.39
CB	Cabañita	Hot spring	315388	5812032	2055	73.6	2.21
COP-2	-	Well cond	314918	5811238	2075	92	8.5

Sample

LM
TC
LMM
AF
CB
COP-2

n.d. = not determined

IB = Ionic balance

Conductivity	Na	Ca	Mg	K	Cl	HCO3	CO3	SO4	SiO2
$\mu\text{S/cm}$	mg/L	mg/L	mg/L	mg/L	mg/L	mg/L	mg/L	mg/L	mg/L
	23.0	20.0	12.2	39.1	35.453	61	30	48	
2580	4.17	11.5	4.28	2.60	2.42	n.d.	n.d.	496	54.02
503	27.0	34.7	11.7	16.80	1.62	166.7	n.d.	102	108.0
11730	26.0	47.5	15.8	30.9	0.35	n.d.	n.d.	4055	369.0
3120	10.0	37.4	9.35	8.38	4.87	n.d.	n.d.	1010	179.0
12750	6.75	9.49	5.85	2.13	0.61	n.d.	n.d.	6515	324.0
79	1.24	0.201	0.043	0.43	0.90	33.3	2.5	0.81	2.40
	Fe	Al	Mn	Si	Li	Rb	Sr	Ba	Cs
	mg/L	mg/L	mg/L	mg/L	$\mu\text{g/L}$	$\mu\text{g/L}$	$\mu\text{g/L}$	$\mu\text{g/L}$	$\mu\text{g/L}$
	22.34	8.99	27	7					
	4.23	5.68	0.14	25.36	3.51	8.39	64.03	32.10	0.38
	0.24	0.03	0.12		31.40	45.10	245.00	70.90	2.51
	87.47	182.01	1.56	172.50	13.50	128.00	228.00	43.30	5.29
	22.88	50.01	0.32	83.68	6.00	30.30	374.00	68.70	2.65
	253.50	756.26	3.53	151.50	60.90	219.00	31.20	0.65	24.00
	0.03	0.03	0.01	1.12	0.09	0.48	0.73	0.29	0.02

F	B	IB
mg/L	mg/L	%
18.99	3.6	
0.18	5.50	9.71
0.08	0.05	-6.24
0.66	0.51	-11.43
0.21	0.02	10.03
0.54	n.d.	-4.25
<0.03	0.001	-

As	Cr	Ni
µg/L	µg/L	µg/L
0.67	1.67	1.53
n.d.	n.d.	0.86
7.17	23.70	8.20
1.98	37.50	7.39
11.40	88.30	33.60
0.31	4.27	0.59

Table 2. Isotopic composition of water, Sr, CO₂, He together with ³H and ¹⁴C activity in thermal water

Sample	Type	$\delta^2\text{H}$	\pm	$\delta^{18}\text{O}$	\pm	$\delta^{18}\text{O}$	$\delta^{13}\text{C-CO}_2$	\pm	$\delta^{18}\text{O-CO}_2$
		‰, SMOW		‰, SMOW		CO ₂ -corrected	‰, PDB		‰, PDB
LM	Hot spring	-48.2	1.5	0.08	0.10	0.08	-7.71	0.01	5.45
TC	Hot spring	-72.6	1.5	-9.17	0.10	-9.28	-7.56	0.01	-3.31
LMM	Hot spring	-49.8	1.5	-2.31	0.10	-2.86	-7.23	0.01	0.99
AF	Hot spring	-80.7	1.5	-9.72	0.10	-9.72	-7.39	0.01	-3.64
CB	Hot spring	-44.0	1.5	1.07	0.10	0.52	-7.51	0.01	-3.60
COP-2	Well	-55.9	1.5	-3.54	0.10	-3.54	-7.81	0.01	2.27

n.d. = not determined

rs of Copahue.

	\pm $^{87}\text{Sr}/^{86}\text{Sr}$	\pm $^4\text{He}/^{20}\text{Ne}$	\pm R/Ra	\pm Rc/Ra	\pm ^3H	F(^{14}C)	\pm ^{14}C age	\pm					
					TU		yrs BP						
0.05	0.70456	0.00013	471.46	14.14	7.17	0.39	7.17	0.42	n.d.	0.113	0.001	17520	93
0.02	0.70412	0.00003	173.83	5.21	7.35	0.21	7.36	0.26	n.d.	0.185	0.002	13540	80
0.05	0.70404	0.00006	27.17	0.82	8.28	0.18	8.37	0.25	0.80	n.d.	-	n.d.	-
0.02	0.70396	0.00006	38.70	1.16	4.61	0.10	4.64	0.14	n.d.	n.d.	-	n.d.	-
0.02	0.70399	0.00005	7.10	0.21	6.79	0.14	7.06	0.20	0.80	n.d.	-	n.d.	-
0.02	0.70697	0.00039	323.80	9.71	6.43	0.14	6.44	0.19	n.d.	0.165	0.001	14470	69

DIC	DOC
ppm	ppm

0.83	0.33
1.46	0.53
0.43	4.28
0.51	5.18
0.57	14.64
6.79	0.50

Dr. Mariano Agosto, Dr. Franco Tassi, Dr. Thomas Darrah, Dr. Stuart Simmons, Dr. Stefano Caliro,
Dr. Giovanni Chiodini, Dr. Orlando Vaselli, Dr. Alberto Caselli, Dr. Dmitri Rouwet, Dr. Johan
Varekamp

Daniele Tardani: Conceptualization, Methodology, Validation, Investigation, Writing - original draft, Supervision. **Emilie Roulleau:** Project administration, Methodology, Validation, Investigation, Writing - review & editing. **Daniele Pinti:** Conceptualization, Methodology, Investigation, Supervision, Writing - review & editing. **Pamela Pérez-Flores:** Conceptualization, Writing - review & editing. **Linda Daniele:** Writing - review & editing. **Martin Reich:** Resources, Writing - review & editing. **Pablo Sánchez:** Writing - review & editing. **Diego Morata:** Resources, Funding acquisition, Writing - review & editing. **Luc Richard:** Methodology.